# Reaction between linear perfluoroaldehydes and hydroperoxy radical in the atmosphere: Reaction mechanisms, reaction kinetics modelling, and atmospheric implications

Zegang Dong<sup>1,2</sup>, Chaolu Xie<sup>3</sup>, Bo Long<sup>1</sup>

Correspondence to: Bo Long (wwwltcommon@sina.com)

ABSTRACT: Linear perfluoroaldehydes are important products formed in the atmospheric oxidation of industrial fluorinated compounds. However, their atmospheric lifetimes are incompletely known. Here, we employ high level quantum chemistry methods and a dual-level strategy for kinetics to investigate the reactions of C<sub>2</sub>F<sub>5</sub>CHO and C<sub>3</sub>F<sub>7</sub>CHO with HO<sub>2</sub>. Our calculated results unveil almost equal activation enthalpies at 0 K for linear perfluoroaldehyde reaction with HO<sub>2</sub>, indicating that the carbon chain length negligibly influences reaction thermodynamics. The calculated kinetics reveal that vibrational anharmonicity enhance rate constants by a factor of 3–10, while torsional anharmonicity reduces rate constants by 34–55%. Additionally, we also find that the reaction of C<sub>3</sub>F<sub>7</sub>CHO with HO<sub>2</sub> exhibits significant pressure dependence, with transition pressures ranging from 0.026 to 2.3 bar across a temperature range of 190–350 K. Furthermore, our findings also reveal that the reactions of C<sub>2</sub>F<sub>5</sub>CHO and C<sub>3</sub>F<sub>7</sub>CHO with HO<sub>2</sub> radicals dominate over those with OH radicals in Russia, Malaysia, parts of Africa by the calculated results in combination with data based on global atmospheric chemical model simulations. These findings establish chain-length-dependent pressure effects and conformational sampling as critical, previously unrecognized factors in kinetics calculations, providing a framework for modelling complex fluorotelomer transformations and guiding emission mitigation strategies.

# 1. Introduction

15

Poly- and perfluoroalkyl substances (PFASs) are highly fluorinated compounds with long atmospheric lifetimes, which have important influences on global warming potential (GWP) and environmental health.(Ackerman Grunfeld et al., 2024; Rupp et al., 2023; Sznajder-Katarzyńska et al., 2019; Wu et al., 2024) During their degradation in the atmosphere, PFASs undergo complex chemical transformations, leading to the formation of linear perfluoroaldehydes. (Alam et al., 2024; Burkholder et al., 2015; David et al., 2021; Wang et al., 2021, 2024) Linear perfluoroaldehydes (C<sub>n</sub>F<sub>2n+1</sub>CHO) are significant intermediate compounds, which belong to the aldehydes family of PFASs.(Li et al., 2024; Thackray et al., 2020) Chlorofluorocarbons (CFCs) and their temporary replacements, hydrochlorofluorocarbons (HCFCs), hydrofluorocarbons

School of Materials Science and Engineering, Guizhou Minzu University, Guiyang, 550025, China

<sup>&</sup>lt;sup>2</sup>School of Chemistry and Chemistry Engineering, South China University of Technology, Guangzhou, 510006, China

<sup>&</sup>lt;sup>3</sup>College of Physics and Mechatronic Engineering, Guizhou Minzu University, Guiyang, 550025, China

30 (HFCs), and hydrofluoroolefins (HFOs) are the important source of the linear perfluoroaldehydes.(Burkholder et al., 2015; Hurley et al., 2006; Martin et al., 2005; Rand and Mabury, 2017; Wang et al., 2023; Waterland and Dobbs, 2007) For example, under low NO<sub>x</sub> conditions, the reaction of OH radicals with the potential foaming agent CF<sub>3</sub>(CF<sub>2</sub>)<sub>2</sub>CH=CH<sub>2</sub> (HFC-1447fz) leads to the formation of C<sub>3</sub>F<sub>7</sub>CHO.(Jiménez et al., 2016; Yu et al., 2024) Furthermore, the atmospheric chemical processes of linear perfluoroaldehydes are of key importance for determining the atmospheric oxidation of fluorotelomer alcohols (FTOHs).(Antiñolo et al., 2012; Hurley et al., 2004)

Linear perfluoroaldehydes were generally considered to be removed through photochemical reactions (Chiappero et al., 2006; Kelly et al., 2004) and free radical reactions initiated by OH and Cl radicals (Andersen et al., 2004; Chiappero et al., 2010; Wang et al., 2007). Additionally, NO<sub>3</sub> may also contribute to their atmospheric degradation. (Burkholder et al., 2015; Ziemann and Atkinson, 2012) During the daytime, photolysis of linear perfluoroaldehydes was considered to be the dominant removal process for  $C_nF_{2n+1}CHO$ , with estimated atmospheric lifetimes ranging from hours to several days. (Antiñolo et al., 2014; Chiappero et al., 2006) Antiñolo et al. (2014) reported that the photolysis lifetime of C<sub>2</sub>F<sub>5</sub>CHO is expected to be 3.5 hours at 273 K, with the main degradation products of CF<sub>3</sub>CFO and COF<sub>2</sub>. In addition, previous investigations have shown that the length of the carbon chain in  $C_nF_{2n+1}CHO$  significantly affects the quantum yield of photolysis. (Chiappero et al., 2006; Kelly et al., 2004) During the nighttime, the reactions of free radicals with C<sub>n</sub>F<sub>2n+1</sub>CHO were considered to be the major degradation pathways. However, previous studies reported relatively slow rate constants for the reaction between OH and  $C_nF_{2n+1}CHO$  (n=1-4) with the values of  $(6.5 \pm 1.2) \times 10^{-13}$ ,  $(5.57 \pm 0.07) \times 10^{-13}$ ,  $(5.8 \pm 0.6) \times 10^{-13}$ , and  $(6.1 \pm 0.5) \times 10^{-13}$  cm<sup>3</sup> molecule<sup>-1</sup> s<sup>-1</sup>, respectively, at 298 K.(Andersen et al., 2004; Antiñolo et al., 2014; Solignac et al., 2007) This corresponds to a longer atmospheric lifetime > 20 days for these linear perfluoroaldehydes. Moreover, the rate constant of Cl atoms with  $C_nF_{2n+1}$ CHO (n = 1-4) is approximately  $2 \times 10^{-12}$  cm<sup>3</sup> molecule<sup>-1</sup> s<sup>-1</sup>. This value is slightly faster than that of the corresponding OH radical reactions under similar conditions. (Andersen et al., 2004; Sulbaek Andersen et al., 2003) The long atmospheric lifetimes of  $C_nF_{2n+1}CHO$  provide an opportunity for other atmospheric oxidation processes of  $C_nF_{2n+1}CHO$  by other atmospheric oxidants.

HO<sub>2</sub> radicals are of ubiquitous active species in the atmosphere with the concentration being two orders of magnitude higher than that of OH radicals. (Bottorff et al., 2023; Gao et al., 2024a; Sascha et al., 2019; Zhang et al., 2019, 2024a, 2022) Moreover, previous investigations have shown that the reactions of aldehydes with HO<sub>2</sub> affect the degradation process of aldehydes. (Hermans et al., 2005; Sascha et al., 2019; Zhou et al., 2024a) Additionally, global three-dimensional chemistry-transport model calculations suggest that the oxidation reactions of formaldehyde and acetone initiated by hydroperoxyl radical contribute to 30% loss of formaldehyde and acetone at the tropical troposphere. (Hermans et al., 2005) Nevertheless, the importance of sink pathway by HO<sub>2</sub> is still unknown because there have not been kinetics data for linear perfluoroaldehydes with HO<sub>2</sub> in the literature. Moreover, chain elongation may have influences on reaction kinetics due to multiple conformers. Furthermore, it is unknown for the pressure-dependent effects of larger perfluoroaldehydes with HO<sub>2</sub>. Although our previous investigations have revealed the importance of CF<sub>3</sub>CHO + HO<sub>2</sub> in the atmosphere (Long et al., 2022), their kinetics of larger perfluoroaldehydes with HO<sub>2</sub> are further required to investigate due to the unique features that depend on the specific reaction

systems such as multi-structural anharmonicity and pressure effects in these complex systems. Additionally, it is a big challenge for addressing the larger perfluoroaldehydes with HO<sub>2</sub> because the computational cost grows very rapidly with system size, making such calculations impractical for high-level quantum chemistry methods.

In this article, we have investigated the reactions of HO<sub>2</sub> with linear perfluoroaldehydes C<sub>n</sub>F<sub>2n+1</sub>CHO (n = 2-5), specifically focusing on C<sub>2</sub>F<sub>5</sub>CHO and C<sub>3</sub>F<sub>7</sub>CHO, referred to as reactions (R1) and (R2) respectively. To delve into these reactions, high-level quantum chemistry calculation close to CCSDT(Q) accuracy in conjunction with dual-level strategy were performed to obtain their quantitative kinetics. Simultaneously, to provide further insight into kinetics, we detailly evaluated the impact of various parameters, including torsional anharmonicity, anharmonicity on the reaction kinetics over atmosphere-related temperatures and pressures. In addition, the chemical transformation of the formed intermediate products has been discussed in reactions R1 and R2. We further estimate the enthalpies of activation at 0 K for the larger-sized reactions of longer-chain perfluoroaldehyde with HO<sub>2</sub>. Moreover, we also discuss the importance of these reactions R1 and R2 by combining the calculated reaction kinetics with global atmospheric modelling. The current results not only provide a comparative analysis with the kinetics of analogous OH-initiated reactions and photolytic processes, but also extend our understanding of the role of HO<sub>2</sub> in modulating the atmospheric lifetime of linear perfluoroaldehydes. This study not only resolves the knowledge gap regarding HO<sub>2</sub>-initiated oxidation of linear perfluoroaldehydes but also establishes a computational strategy for predicting the atmospheric fates of long-chain PFAS derivatives. Our findings provide critical insights for refining emission control strategies and mitigating the environmental persistence of these compounds.

$$C_2F_5CHO + HO_2 \rightarrow C_2F_5CH(OH)OO$$
 (R1)

$$C_3F_7CHO + HO_2 \rightarrow C_3F_7CH(OH)OO$$
 (R2)

#### 2. Computational methods and atmospheric modelling

70

80

85

## 2.1 Options for electronic structure density functionals

Our goal is to establish a precise set of electronic structure and kinetic calculation methods for the XCHO + HO<sub>2</sub> reaction, delivering satisfactory quantitative results.(Long et al., 2022) This previous study indicated that the CCSD(T)-F12a/cc-pVTZ-F12/M06-2X/MG3S theoretical methods can make good agreement with beyond-CCSD(T) results for the similar reaction of HCHO + HO<sub>2</sub>.(Long et al., 2022) Furthermore, CCSD(T)-F12a/cc-pVTZ-F12 has been shown good performance for molecules containing fluorine atoms.(Dong et al., 2021; Long et al., 2022; Xia et al., 2024) Consequently, we intend to utilize the well-validated methods in the present investigations in reactions R1 and R2. Specifically, the M06-2X(Zhao and Truhlar, 2008b, a) density functional with the MG3S(Lynch et al., 2003) basis set was employed to optimize the geometries, while CCSD(T)-F12a(Adler et al., 2007; Knizia et al., 2009)/cc-pVTZ-F12 for R1 and R2 and FNO-CCSD(T)-F12(Gyevi-Nagy et al., 2021; Taube and Bartlett, 2008)/cc-pVDZ-F12 for other C<sub>n</sub>F<sub>2n+1</sub>CHO + HO<sub>2</sub> (n = 1 - 5) were used to calculate single-point energies. The FNO-CCSD(T) approach that significantly improves computational efficiency with cost reduction of up to an order of

magnitude was utilized to calculate larger systems. Furthermore, intrinsic reaction coordinate (IRC) calculation was done to determine the correct transition states by examining the connections of each saddle point to its corresponding minima.(Hratchian and Schlegel, 2004, 2005; Kenyon, 1968)

# 2.2 Vibrational frequencies

We found that standard scale factor is actually not applicable for some transition states in previous investigation, so we used two scale factors.(Zheng et al., 2014, 2015) The standard scale factor for M06-2X/MG3S is 0.970. Furthermore, we also calculated the specific reaction scale factors to assess the effects of anharmonicity. The reaction-specific scale factors were obtained by using the MPW1K/6-311+G(2df, 2p) electronic structure method based on the hybrid degeneracy-corrected second-order vibrational perturbation theory (HDCVPT).(Bloino et al., 2012; Kuhler et al., 1996) This is necessary and effective for eliminating the activation enthalpy error caused by the standard scale factors and the results were list in Table S1 and Table S2, Supplement. This was obtained by equation (1),

$$\lambda^{SRP,ZPE} = \lambda^{Anh} \lambda^{H} \tag{1}$$

where  $\lambda^{Anh}$  is the ratio of anharmonic zero-point vibrational energies (ZPE) to harmonic ZPE at the MPW1K/6-311+G(2df, 2p) level.  $\lambda^{H}$  is 0.983 for M06-2X/MG3S to correct harmonic frequencies. The result shows that the specific reaction scale factors are 0.955 for TS1 (See Table S1) and 0.956 for TS2 (See Table S1), which is a large deviation from the standard value of 0.970; this results in a decrease in calculated enthalpies of activation of 0.72 and 0.78 for TS1 and TS2 at 0 K, respectively. In addition, multi-structural torsional anharmonicity involving reactant and transition state were all calculated using MS-T method (multi-structural method for torsional anharmonicity).(Yu et al., 2012; Zheng et al., 2011; Zheng and Truhlar, 2013)

## 2.3 kinetics calculations

110

115

120

The dual-level strategy was utilized to compute the high-pressure limit rate constant. (Long et al., 2016, 2019; Xia et al., 2024) As shown in equation (2), we integrated a conventional transition-state theory rate constant  $k_{TST}^{HL}$  predicated on higher-level (HL, CCSD(T)-F12a/cc-pVTZ-F12//M06-2X/MG3S) inputs with transmission coefficients derived from direct dynamics at a lower level (LL, M11-L/MG3S), employing a specific density functional that is chose from the results of benchmark calculations (see Table S3). We have incorporated both a recrossing transmission coefficient  $\Gamma_{CVT/TST}^{LL}$  and a tunneling transmission coefficient  $k_{SCT}^{LL}$ , as calculated through reaction-path variational transition state theory, with a particular emphasis on the canonical variational theory coupled with small-curvature tunneling (CVT/SCT).(Garrett and Truhlar, 1979; Liu et al., 1993; Truhlar et al., 1982) Additionally, a multi-structural transmission coefficient ( $F^{MS-T}$ ) was introduced to this framework to cancel the errors caused by the multi-structural anharmonicity, thereby advancing our approach to the DL-MS-CVT/SCT method, which provides a detailed and multifaceted treatment of the rate constant calculation, and can effectively obtain quantitative kinetics.

125  $k_{MS-CVT/SCT}^{DL} = F^{MS-T} \times k_{TST}^{HL} \times k_{SCT}^{LL} \times \Gamma_{CVT/TST}^{LL}$  (2)

The pressure-dependent rate constants were done by employing the system-specific quantum Rice-Ramsperger-Kassel (SS-QRRK) theory in the temperature range of 190-350 K.(Bao et al., 2016b, a; Bao and Truhlar, 2017) This method relies only on the high-pressure limiting rate constant that was calculated by the dual-level strategy. The computational details of pressure-dependent rate constants are presented in the Supplement.

# 130 **2.4 Atmospheric modelling**

We used GEOS-Chem 14.4.2 with a horizontal resolution of 2.0° × 2.5° to simulate space distribution of HO<sub>2</sub> and OH at 47 vertical layers in the period from February 2018 to February 2019.(Bey et al., 2001) The time includes six months of spin-up and output per hour. GEOS-Chem is a global, three-dimensional chemical transport model associated with atmospheric composition (http://geos-chem.org). Modern-Era Retrospective analysis for Research and Applications, Version 2 (MERRA-2)(Gelaro et al., 2017) was used as meteorological field data and Harmonized Emissions Component (HEMCO 3.9) was used as the source of emissions data.(Lin et al., 2021) The emissions include biogenic emissions from Model of Emissions of Gases and Aerosols from Nature (MEGANv2.1)(Hu et al., 2015; McDuffie et al., 2020) and anthropogenic emissions from the global Community Emissions Data System (CEDS) (McDuffie et al., 2020) inventory. Simulation uses default full chemistry mechanism including HO<sub>x</sub>-NO<sub>x</sub>-VOC-O<sub>3</sub>-halogen chemistry, which is done by our previous investigation.(Bloss et al., 2007)

# 140 **2.5 Software**

135

145

All density function calculation, including Zero-point energy (ZPE) correction were carried out using Gaussian 16 software package, (Zhao and Truhlar, 2008b) and the single point energy calculations for CCSD(T)-F12a/cc-pVTZ-F12 and FNO-CCSD(T)-F12a/cc-pVDZ-F12 were done using Molpro 2019 (Werner et al., 2019) and MRCC code. (Kállay et al., 2020; M. Kállay, P. R. Nagy, D. Mester, L. Gyevi-Nagy, J. Csóka, P. B. Szabó, Z. Rolik, G. Samu, J. Csontos, B. Hégely, Á. Ganyecz, I. Ladjánszki, L. Szegedy, B. Ladóczki, K. Petrov, M. Farkas, P. D. Mezei, 2022) MS-T method was executed through MSTor-2023 program package. (Chen et al., 2023) The rate constants were done with the KiSThelP, (Canneaux et al., 2014) Polyrate 2017-C, and Gaussrate 2017-B. (Zheng et al., 2017, n.d.)

## 3. Results and discussion

## 3.1. The electronic structure of the C<sub>2</sub>F<sub>5</sub>CHO/C<sub>3</sub>F<sub>7</sub>CHO + HO<sub>2</sub> reaction

We considered the C<sub>2</sub>F<sub>5</sub>CHO/C<sub>3</sub>F<sub>7</sub>CHO + HO<sub>2</sub> reaction similar to the reactions of aldehydes with HO<sub>2</sub>.(Long et al., 2022) The dominant mechanism is that the hydrogen atom of HO<sub>2</sub> is transferred to the terminal oxygen atom of C<sub>2</sub>F<sub>5</sub>CHO/C<sub>3</sub>F<sub>7</sub>CHO, and simultaneously, the oxygen atom of HO<sub>2</sub> is connected to carbon atom of carbonyl group of C<sub>2</sub>F<sub>5</sub>CHO/C<sub>3</sub>F<sub>7</sub>CHO. Figure 1

depicts ZPE corrected potential energy profile of the reaction of  $C_2F_5CHO/C_3F_7CHO + HO_2$  at the CCSD(T)-F12a/cc-pVTZ-F12//M06-2X/MG3S level.  $C_2F_5CHO/C_3F_7CHO$  and  $HO_2$  form reaction complexes RC1/RC2, and then pass through transition

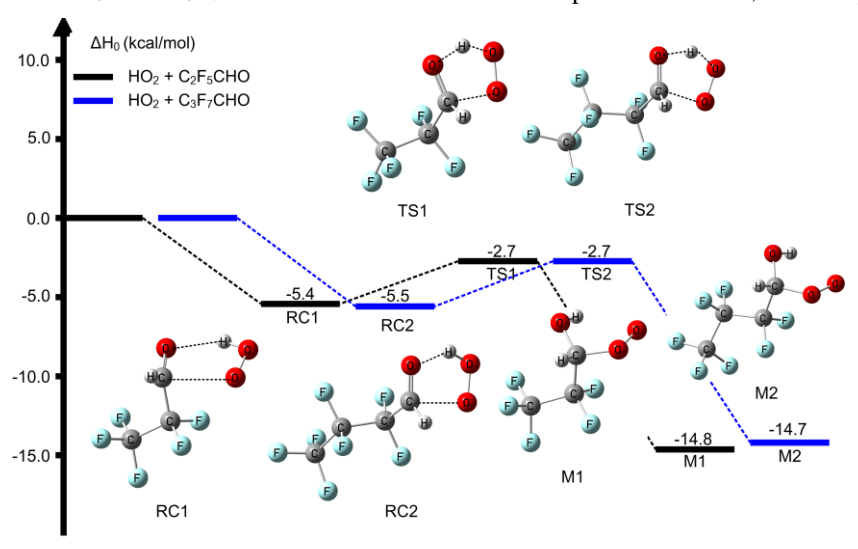


Figure 1. Enthalpy profile of the  $HO_2$  addition reaction with  $C_2F_5CHO$  and  $C_3F_7CHO$  as calculated by CCSD(T)-F12a/cc-pVTZ-F12//M06-2X/MG3S level with the scale factor by the standard method at 0~K.

155

160

165

170

175

states TS1 and TS2 to form the intermediate products of  $C_2F_5CH(OH)OO$  (M1) and  $C_3F_7CH(OH)OO$  (M2), respectively. TS1 (-2.7 kcal/mol) denotes the global minimum optimized structures of the stationary points of enthalpy of activation at 0 K; this is 0.3 kcal/mol and 1.6 kcal/mol lower than that of the  $CF_3CHO + HO_2$  and  $CH_3CHO + HO_2$  reactions, respectively. (Long et al., 2022) This shows that the reaction of perfluoroaldehydes with  $HO_2$  may be kinetically feasible. As a comparison, the further energy profile of the  $C_3H_7CHO + HO_2$  reaction shows an equal enthalpy of activation of -2.7 kcal/mol for TS2; this is slightly lower than that of enthalpy of activation -2.4 kcal/mol for the reaction of  $CF_3CHO + HO_2$ . (Gao et al., 2024b)

It is noteworthy that Figure 1 only depicts the potential energy profile of the reaction featuring the global minimum structure. Nevertheless, the internal rotation of the C–C bond produces multiple conformers for reactants, transition states, and formed intermediate products. Their geometric configurations and energy distributions relative to the global minimum structure are presented in Figure S1. Regarding the reactions of C<sub>2</sub>H<sub>3</sub>CHO and C<sub>3</sub>H<sub>7</sub>CHO with HO<sub>2</sub>, we have observed that as the carbon chain lengthens, the number of conformers of both reactants and transition states increases, and the energy distribution broadens. For instance, TS1 has three isomers, with an energy distribution spanning from 0 to 1.7 kcal/mol, whereas TS2 has five isomers, and its energy distribution ranges from 0 to 1.9 kcal/mol. In terms of geometric configurations, the low-energy isomers tend to have more linear structures, while the high-energy conformations exhibit more pronounced curling.

NO is a highly reactive gas. (Lee et al., 2024) Human activities, especially agriculture and industrial processes, have led to significant NO emissions. (Andersen et al., 2024; Thomson et al., 2012) Industrial activities contribute to NO levels such as fossil fuel combustion in power plants and chemical manufacturing, along with vehicle emissions. Given its prevalence from human-induced emissions, we further explore the degradation pathways of intermediate products M1 and M2 in the presence

of NO. As depicted in Figure S2, M1 and M2 undergo initial reactions with NO to yield the products C<sub>2</sub>F<sub>5</sub>CH(O)OH, C<sub>3</sub>F<sub>7</sub>CH(O)OH, and NO<sub>2</sub>, exhibiting activation enthalpies of –9.9 and –11.5 kcal/mol at 0 K, respectively. These results are consistent with previous studies on similar reactions involving RO<sub>2</sub> + NO. (Berndt et al., 2015; King et al., 2001; Nie et al., 2023; Orlando et al., 2000; Vereecken and Peeters, 2009) These products then undergo unimolecular reactions to decompose into C<sub>2</sub>F<sub>5</sub> and C<sub>3</sub>F<sub>7</sub> radicals and formic acid in Figure 2. Notably, the unimolecular decomposition of C<sub>2</sub>F<sub>5</sub>CH(O)OH and C<sub>3</sub>F<sub>7</sub>CH(O)OH represents the rate-determining step of the overall reaction, with corresponding activation enthalpies of 5.6 kcal/mol and 4.7 kcal/mol (0 K), respectively; this indicates that formic acid may potentially be formed via C<sub>2</sub>F<sub>5</sub>CHO/C<sub>3</sub>F<sub>7</sub>CHO + HO<sub>2</sub> in the presence of high concentration NO in the atmosphere. Additionally, the formed intermediate products (M1 and M2) are a typical class of RO<sub>2</sub> radicals. In the low NO<sub>x</sub> levels, these RO<sub>2</sub> radicals can also participate in bimolecular reactions. (Ding and Long, 2022) RO<sub>2</sub> can react with HO<sub>2</sub>, resulting in the formation of the stable product ROOH. Moreover, RO<sub>2</sub> can react with other RO<sub>2</sub> or R'O<sub>2</sub> (where R' denotes a hydrocarbon fragment). (Bottorff et al., 2023) The reaction with R'O<sub>2</sub> frequently yields alkoxy radicals, and both of these reactions are capable of producing stable products. (Goldman et al., 2021) Due to the complexity of these bimolecular reactions of the formed RO<sub>2</sub> in the reactions R1 and R2, we did not further investigate their reaction mechanisms and kinetics in the present work.

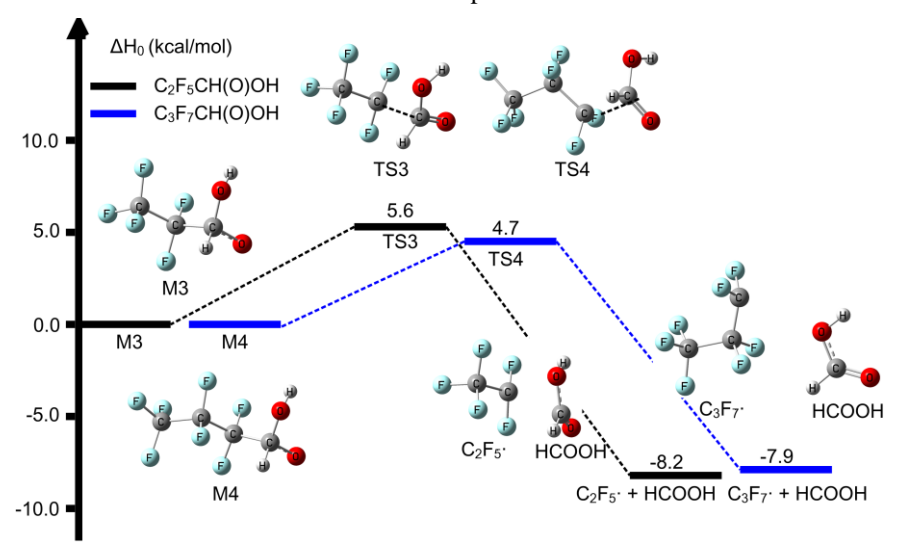


**Figure 2.** Relative enthalpies at 0 K for the decomposition of C<sub>2</sub>F<sub>5</sub>CH(O)OH (M3) and C<sub>3</sub>F<sub>7</sub>CH(O)OH (M4) calculated by CCSD(T)-F12a/cc-pVTZ-F12//M06-2X/MG3S.

We further conducted an extended study on the reactions of C<sub>4</sub>F<sub>9</sub>CHO and C<sub>5</sub>F<sub>11</sub>CHO at the FNO-CCSD(T)-F12//cc-pVDZ-F12//M06-2X/MG3S level, aiming to investigate the effects of increasing carbon chain length on the enthalpy of activation at 0 K. The calculated results show a deviation of only 0.2 kcal/mol in activation enthalpy at 0 K between FNO-CCSD(T)-F12//cc-pVDZ-F12 (-2.6 kcal/mol) and CCSD(T)-F12a/cc-pVTZ-F12 (-2.4 kcal/mol) in CF<sub>3</sub>CHO + HO<sub>2</sub>, validating the robustness of FNO-CCSD(T)-F12//cc-pVDZ-F12 for complex fluorinated systems. Data from Figure 3 reveal an interesting phenomenon that the activation enthalpy at 0 K remains almost equal C2 (C<sub>2</sub>F<sub>5</sub>CHO) to C5 (C<sub>5</sub>F<sub>11</sub>CHO). This

finding aligns with the similar trend for the reaction of  $C_nH_{2n+1}CHO$  with  $HO_2$ , suggesting that the impact of carbon chain length growth on the enthalpy of activation at 0 K is quite minor.(Ding and Long, 2022; Gao et al., 2024b) However, the introduction of  $CF_3$  leads to a relatively lower enthalpy of activation at 0 K for the  $C_nH_{2n+1}CHO + HO_2$  reactions, primarily due to the strong electron-withdrawing ability of fluorine atoms, which can stabilize the transition

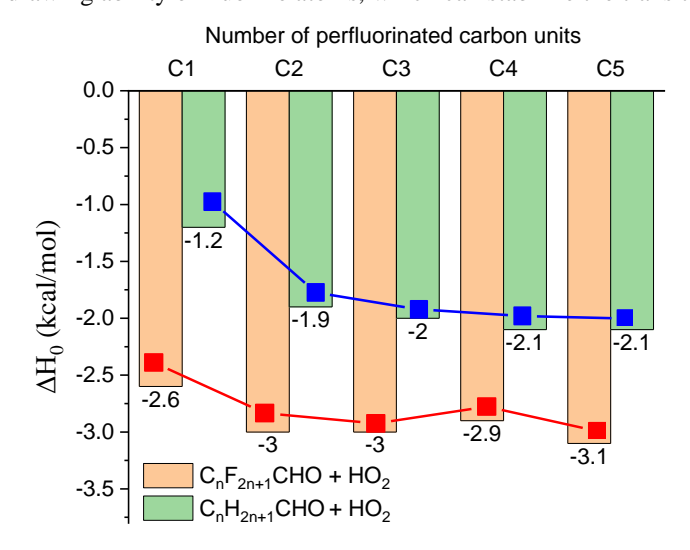


Figure 3. The impacts of perfluorinated carbon length on the enthalpies of activation at 0 K in the C<sub>n</sub>H<sub>2n+1</sub>CHO/C<sub>n</sub>F<sub>2n+1</sub>CHO + HO<sub>2</sub> reactions.

The values for C<sub>n</sub>H<sub>2n+1</sub>CHO (n = 1-5) + HO<sub>2</sub> and C<sub>n</sub>F<sub>2n+1</sub>CHO + HO<sub>2</sub> are obtained from references (Ding and Long, 2022; Gao et al., 2024a) and calculated by using FNO-CCSD(T)-F12a/cc-pVDZ-F12.

state and lower the enthalpy of activation at 0 K. As the size of perfluoroaldehyde increases, the multi-structure effects caused by torsion of C-C bonds become more pronounced. The relative energy values of reactants and transition states shown in Figure S1 and S3 (relative to the global minimum energy value, without ZPE correction) indicate that with increasing molecular size, the number of possible isomers increases, leading to a broader energy distribution. For instance, C<sub>2</sub>F<sub>5</sub>CHO exhibits three transition state conformers with energy differences spanning 0–1.7 kcal/mol, while C<sub>3</sub>F<sub>7</sub>CHO has five conformers distributed over 0–1.8 kcal/mol. This trend amplifies for longer chains: C<sub>5</sub>F<sub>11</sub>CHO generates 36 distinct conformers in its transition state, with energy variations extending up to 4.8 kcal/mol. This broad energy distribution has significant implications for the thermodynamics and kinetics of the degradation process of perfluoroaldehydes, potentially increasing the diversity and complexity of reaction pathways.

# 3.2. Kinetics of C<sub>2</sub>F<sub>5</sub>CHO/C<sub>3</sub>F<sub>7</sub>CHO + HO<sub>2</sub>

200

210

215

220

The high-pressure limiting rate constants were calculated for the temperature range of 190-350 K, covering a wide atmospheric temperature range. For the reactions  $C_2F_5CHO + HO_2$  (R1) and  $C_3F_7CHO + HO_2$  (R2), the rate constants incorporating multi-structure anharmonicity corrections are defined as  $k_1$  and  $k_2$ , respectively. According to Zheng (Zheng and Truhlar, 2010), the rate constants at high pressure are fitted using equation (3).

$$k = A \left(\frac{T + T_0}{300}\right)^n \exp\left[-\frac{E(T + T_0)}{R(T^2 + T_0^2)}\right]$$
 (3)

Table S4 lists the fitting parameters A, n, E, and  $T_0$ . Here, T represents temperature in Kelvin, and R is the ideal gas constant  $(0.0019872 \text{ kcal mol}^{-1} \text{ K}^{-1})$ . The temperature-dependent Arrhenius activation energies are determined from the fits using equation (4).

$$225 E_0 = -R \frac{d \ln k}{d(1/T)} (4)$$

The high-pressure limit rate constants, incorporating multiple-structure anharmonicity torsional corrections, are illustrated in Figure 4, with more comprehensive data provided in Tables S5-S7. Regarding the  $C_2F_5CHO + HO_2$  reaction, the rate constant  $k_1$  exhibits a decrease from  $3.35 \times 10^{-12}$  cm³ molecule<sup>-1</sup> s<sup>-1</sup> at 190 K to  $5.42 \times 10^{-14}$  cm³ molecule<sup>-1</sup> s<sup>-1</sup> at 350 K in Figure 4 and Tables S5-S7. Similarly, the rate constant  $k_2$  for the  $C_3F_7CHO + HO_2$  reaction also decreases with increasing temperature. These trends are consistent with theoretical studies of non-fluorinated aldehydes such as  $C_2H_5CHO$  and  $C_3H_7CHO$ , where rate constants for reactions with  $HO_2$  were reported in the range of  $10^{-14}$  to  $10^{-13}$  cm³ molecule<sup>-1</sup> s<sup>-1</sup> at atmospheric temperatures, indicating similar reactivity between fluorinated and non-fluorinated aldehydes with  $HO_2$ .(Ding and Long, 2022; Gao et al., 2024a)

230

240

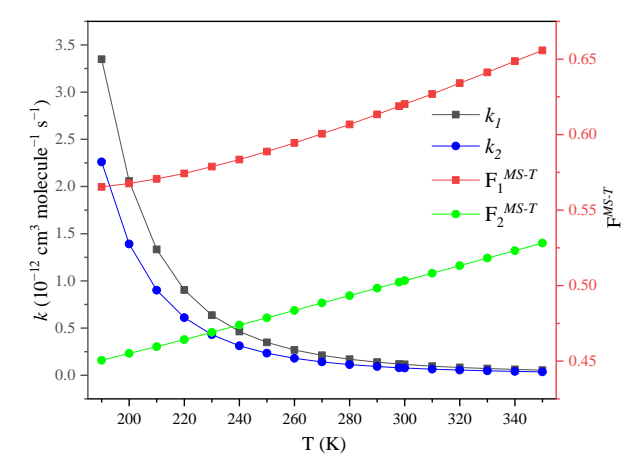


Figure 4. The high-pressure limit rate constants of the reactions of C<sub>2</sub>F<sub>5</sub>CHO and C<sub>3</sub>F<sub>7</sub>CHO with HO<sub>2</sub> at the temperature range of 190–350 K.

In addition, the effects of recrossing and multi-structural anharmonicity are quite limited, approximately ranging between 0.4 and 0.7 times. This results in the rate constants for reactions R1 and R2 being 2-3 times slower than that of  $CF_3CHO + HO_2$ . For instance, the rate constants of  $C_2F_5CHO + HO_2$  and  $C_3F_7CHO + HO_2$  are estimated to be  $1.19 \times 10^{-13}$  and  $7.92 \times 10^{-14}$  cm<sup>3</sup> molecule<sup>-1</sup> s<sup>-1</sup> at 298 K, respectively, which is slow by compared to  $2.48 \times 10^{-13}$  cm<sup>3</sup> molecule<sup>-1</sup> s<sup>-1</sup> of  $CF_3CHO + HO_2$ . (Long et al., 2022) Moreover, the effect of anharmonicity in vibrational-frequency scale factors on high pressure limited rate constants were further discussed. We define "f" as the ratio between the rate constant calculated using the reaction-specific vibrational-frequency scale factors and that calculated using the standard vibrational-frequency scale factors. As depicted in Figure 5, the

rate constants obtained using the reaction-specific scale factors are 3-7 and 4-10 times fast compared to those calculated using the standard scale factors. Consequently, employing reaction-specific scale factors is crucial for accurate rate calculations.

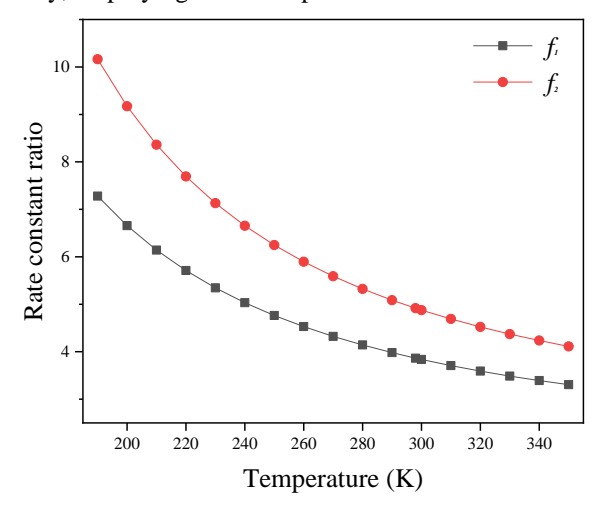


Figure 5. The ratio between the rate constant calculated using the reaction-specific vibrational-frequency scale factors and the rate constant calculated using the standard vibrational-frequency scale factors, within the temperature range of 190–350 K.  $f_1$  and  $f_2$  represent the ratios for the reactions of  $C_2F_5CHO + HO_2$  and  $C_3F_7CHO + HO_2$ , respectively.

250

255

The pressure-dependent rate constants of the HO<sub>2</sub> reaction with C<sub>2</sub>F<sub>5</sub>CHO and C<sub>3</sub>F<sub>7</sub>CHO were further calculated by using SS-QRRK method. As shown in Figure 6-7 and Table S8-S9, it can be observed that variations of the calculated rate constant with respect to pressure have a minimal impact on the rate constant of C<sub>2</sub>F<sub>5</sub>CHO + HO<sub>2</sub>, indicating the absence of significant pressure effects. However, significant pressure effects are observed in the C<sub>3</sub>F<sub>7</sub>CHO + HO<sub>2</sub> reaction, particularly at temperatures above 300 K. To provide a clearer perspective, we define the transition pressure  $p_{1/2}$  to quantify the pressure dependence. Specifically, the transition pressure  $p_{1/2}$  is the pressure at which the pressure-dependent rate constant reaches half of its high-pressure limit. Figure 8 and Table S10 show that the transition pressure  $p_{1/2}$  for the HO<sub>2</sub> + C<sub>2</sub>F<sub>5</sub>CHO reaction ranging from  $2.6 \times 10^{-5}$  to  $7.4 \times 10^{-3}$  bar at 190-350 K, while the transition pressure  $p_{1/2}$  ranges from  $2.6 \times 10^{-2}$  to 2.3 bar at 190-350 K for the HO<sub>2</sub> + C<sub>3</sub>F<sub>7</sub>CHO reaction. This indicates that the HO<sub>2</sub> + C<sub>3</sub>F<sub>7</sub>CHO reaction exhibits a significant pressure dependence, and the increase in carbon chain length has a significantly affect pressure-dependent rate constants.

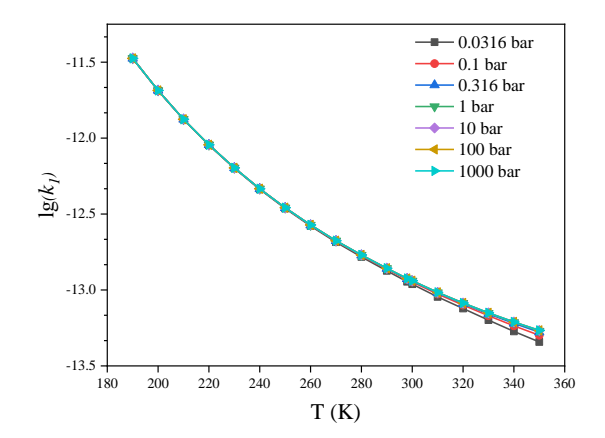


Figure 6. Pressure-dependent rate constants of C<sub>2</sub>F<sub>5</sub>CHO + HO<sub>2</sub> as functions of temperature obtained via the SS-QRRK method.

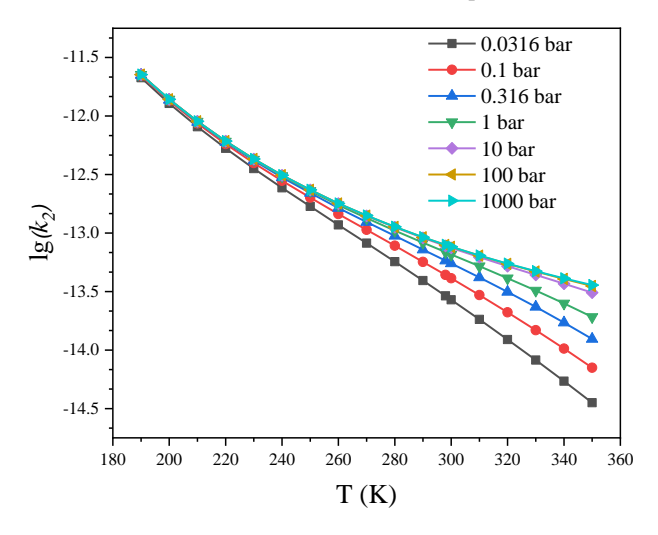


Figure 7. Pressure-dependent rate constants of C<sub>3</sub>F<sub>7</sub>CHO + HO<sub>2</sub> as functions of temperature obtained via the SS-QRRK method.

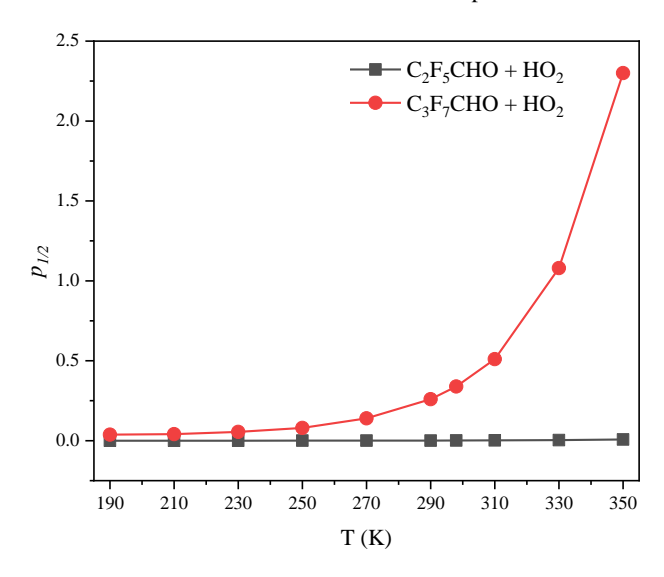


Figure 8. Transition pressure  $p_{1/2}$  calculated by the SS-QRRK method for the HO<sub>2</sub> + C<sub>2</sub>F<sub>5</sub>CHO and HO<sub>2</sub> + C<sub>3</sub>F<sub>7</sub>CHO reactions as functions of temperature.

## 3.3. Atmospheric Implications.

270

275

Given that the reaction of OH +  $C_2F_5CHO/C_3F_7CHO$  was considered to be the main sink for  $C_2F_5CHO/C_3F_7CHO$ , it is necessary to establish the competitive relationship between OH +  $C_2F_5CHO/C_3F_7CHO$  and  $HO_2+$   $C_2F_5CHO/C_3F_7CHO$ . Therefore, we have defined the ratio of rate between them according to the equations (5) and (6).

$$v_1 = \frac{k_1[C_2F_5CHO][HO_2]}{k_{OH}[C_2F_5CHO][OH]}$$
(5)

$$v_2 = \frac{k_2[C_3F_7CHO][HO_2]}{k'_{OH}[C_3F_7CHO][OH]}$$
(6)

Here,  $k_1$  and  $k_2$  are the rate constants of HO<sub>2</sub> + C<sub>2</sub>F<sub>5</sub>CHO and HO<sub>2</sub> + C<sub>3</sub>F<sub>7</sub>CHO calculated by this work, respectively, while  $k_{\rm OH}$  and  $k'_{OH}$  are the corresponding rate constants of OH+ C<sub>2</sub>F<sub>5</sub>CHO and OH + C<sub>3</sub>F<sub>7</sub>CHO, from the literature (Solignac et al., 2007; Wang et al., 2007). We calculated the rate ratios using a high OH concentration(Lew et al., 2020) of 5 × 10<sup>6</sup> molecules cm<sup>-3</sup> and a typical HO<sub>2</sub> concentration(Brasseur and Solomon, 2006) of 1.4 × 10<sup>8</sup> molecules cm<sup>-3</sup>. The calculations presented in Table 1 reveal that within the temperature range of 240-350 K, the rate ratios for  $v_1$  and  $v_2$  are in the

**Table 1.** Rate ratios of  $HO_2 + C_2F_5CHO$  to  $OH + C_2F_5CHO$  and  $HO_2 + C_3F_7CHO$  to  $OH + C_3F_7CHO$  within the Temperature Range of 240 to 350 K.

T(K)	$k_{OH}{}^a$	$k_{OH}^{\prime}{}^{a}$	${v_1}^b$	$v_2{}^b$
240	$3.80 \times 10^{-13}$	$4.30 \times 10^{-13}$	34.22	20.34
250	$4.10\times10^{\text{-}13}$	$4.57\times10^{\text{-}13}$	23.80	14.31
260	$4.40\times10^{\text{-}13}$	$4.84\times10^{\text{-}13}$	17.09	10.38
270	$4.69 \times 10^{-13}$	$5.10\times10^{\text{-}13}$	12.6	7.74
280	$4.99\times10^{\text{-}13}$	$5.35\times10^{\text{-}13}$	9.55	5.90
290	$5.28\times10^{\text{-}13}$	$5.60\times10^{\text{-}13}$	7.36	4.60
298	$5.51 \times 10^{-13}$	$5.80 \times 10^{-13}$	6.06	3.83
310	$5.84\times10^{\text{-}13}$	$6.08\times10^{\text{-}13}$	4.62	2.96
320	$6.12 \times 10^{-13}$	$6.31 \times 10^{-13}$	3.76	2.43
330	$6.39\times10^{\text{-}13}$	$6.54 \times 10^{-13}$	3.10	2.02
340	$6.66\times10^{\text{-}13}$	$6.76\times10^{\text{-}13}$	2.59	1.70
350	$6.92\times10^{-13}$	$6.97\times10^{\text{-}13}$	2.19	1.45

<sup>&</sup>lt;sup>a</sup>**k**<sub>0H</sub> and **k**'<sub>0H</sub> are the rate constants of the OH reactions with C<sub>2</sub>F<sub>5</sub>CHO and C<sub>3</sub>F<sub>7</sub>CHO, from the literature(Antiñolo et al., 2014; Solignac et al., 2007) respectively. <sup>b</sup>**v**<sub>1</sub> and **v**<sub>2</sub> denote the rate ratios of HO<sub>2</sub> with C<sub>2</sub>F<sub>5</sub>CHO and C<sub>3</sub>F<sub>7</sub>CHO to OH with C<sub>2</sub>F<sub>5</sub>CHO and C<sub>3</sub>F<sub>7</sub>CHO, respectively.

range of 34.22 to 2.19 and 20.34 to 1.45, respectively. These substantial findings indicate that the reactions of HO<sub>2</sub> with C<sub>2</sub>F<sub>5</sub>CHO and C<sub>3</sub>F<sub>7</sub>CHO can dominate the removal of these compounds, comparing with the corresponding OH reactions, thereby exerting a substantial impact on their elimination processes. We also determined the rate constants governing the reactions of C<sub>2</sub>F<sub>5</sub>CHO and C<sub>3</sub>F<sub>7</sub>CHO with HO<sub>2</sub> within the altitude range of 0-50 km, and subsequently evaluated the atmospheric lifetimes of these compounds. The HO<sub>2</sub>-mediated elimination pathways for C<sub>2</sub>F<sub>5</sub>CHO and C<sub>3</sub>F<sub>7</sub>CHO are characterized by relatively rapid reaction rates within the troposphere (< 10 km), resulting in relatively short atmospheric lifetimes of approximately 14.4 - 31.3 hours and 21.6 - 51.8 hours (See Table 2). These atmospheric lifetimes are considerably shorter than the 20-day atmospheric lifetime estimated for the reactions involving OH radicals with C<sub>2</sub>F<sub>5</sub>CHO and C<sub>3</sub>F<sub>7</sub>CHO, and even can somewhat shorter than photolysis (one day)(Solignac et al., 2007). This highlights the noteworthy impact of HO<sub>2</sub>-initiated elimination pathways on the atmospheric degradation of these compounds.

285

290

300

**Table 2.** Hydroperoxyl radical concentration (in molecules cm<sup>-3</sup>), rate constants (in cm<sup>3</sup> molecule<sup>-1</sup> s<sup>-1</sup>), and atmospheric lifetimes (in hours) with respect to bimolecular reactions as functions of altitude.

H (km) <sup>a</sup>	T (K) <sup>a</sup>	P (mbar) <sup>a</sup>	$[HO_2]^b$	$k_1(T, p)^c$	$k_2(T, p)^c$	$ au_1{}^d$	$ au_2{}^d$
0	290.2	1010	1.40E+08	1.38E-13	9.18E-14	1.44E+01	2.16E+01
5	250.5	496	4.90E+07	3.44E-13	2.30E-13	1.65E+01	2.47E+01
10	215.6	243	8.30E+06	1.07E-12	6.47E-13	3.13E+01	5.18E+01
15	198	119	2.30E+06	2.21E-12	2.98E-13	5.47E+01	4.05E+02
20	208	58.2	2.90E+06	1.38E-12	1.22E-13	6.93E+01	7.85E+02
25	216.1	28.5	5.70E+06	9.38E-13	4.32E-14	5.20E+01	1.13E+03
30	221.5	13.9	7.50E+06	6.52E-13	1.29E-14	5.68E+01	2.88E+03
35	228.1	6.83	6.90E+06	4.04E-13	4.13E-15	9.96E+01	9.74E+03
40	240.5	3.34	5.90E+06	2.29E-13	1.73E-15	2.06E+02	2.73E+04
45	251.9	1.64	4.90E+06	1.27E-13	6.56E-16	4.45E+02	8.64E+04
50	253.7	0.801	4.00E+06	5.87E-14	1.80E-16	1.18E+03	3.86E + 05

<sup>a</sup>H denotes altitude (atmospheric scale height); T denotes temperature; p denotes pressure. <sup>b</sup>Data are from ref (Brasseur and Solomon, 2006). <sup>c</sup>k<sub>1</sub>, k<sub>2</sub> are the rate constants of the HO<sub>2</sub> reactions with C<sub>2</sub>F<sub>5</sub>CHO and C<sub>3</sub>F<sub>7</sub>CHO, respectively. <sup>d</sup>τ<sub>1</sub> = 1/(k<sub>1</sub>[HO<sub>2</sub>]) and τ<sub>2</sub> = 1/(k<sub>2</sub>[HO<sub>2</sub>]) define the atmospheric lifetimes for HO<sub>2</sub> reactions with C<sub>2</sub>F<sub>5</sub>CHO and C<sub>3</sub>F<sub>7</sub>CHO, respectively.

To provide further insight into the importance of these reactions in the atmosphere, we analyse the concentrations of  $HO_2$  and OH by using Geos-Chem. The concentration of modelled  $HO_2$  reached a maximum of  $4.99 \times 10^8$  molecule cm<sup>-3</sup> in the Amazon region and a mean value of  $9.93 \times 10^7$  molecule cm<sup>-3</sup>.(Long et al., 2024) Simultaneously, the concentrations of  $HO_2$  (1.7 × 10<sup>7</sup> molecule cm<sup>-3</sup>) is consistent with field observations at the British Antarctic Survey's Halley Research Station (1.5 ppt).(Bloss et al., 2007) We also note that there is a maximum concentration of  $8.03 \times 10^6$  molecule cm<sup>-3</sup> over the Atlantic and Pacific oceans and an average concentration of  $1.06 \times 10^6$  molecule cm<sup>-3</sup> for OH.(Lelieveld et al., 2016) Based on the rate ratios calculated above, when the concentration of  $HO_2$  is two orders of magnitude higher than that of OH, the reaction with

HO<sub>2</sub> dominates over the reaction with OH. Therefore, we compare HO<sub>2</sub> and OH concentrations in global regions and find at least a 2-order of magnitude difference in concentrations in industrial parks such as Russia, Malaysia, and parts of Africa (see Figure 9). Specifically, in parts of Africa, HO<sub>2</sub> concentrations are even three orders of magnitude higher than that of OH. Additionally, high HO<sub>2</sub>/OH ratios have been observed along the Indian Ocean margin near Indonesia, which may be attributed to atmospheric transport and enhanced HO<sub>2</sub> production from industrial activities. In the Amazon region, the [HO<sub>2</sub>]/[OH] ratio can reach as high as 410–1,200. This significantly increases the HO<sub>2</sub>-to-OH degradation rate ratios for C<sub>2</sub>F<sub>5</sub>CHO and C<sub>3</sub>F<sub>7</sub>CHO, reaching 88.5–259 and 56.0–164, respectively. These rate ratios indicate that HO<sub>2</sub>-driven degradation exceeds OH-mediated degradation by over 50 times. This large concentration ratios between HO<sub>2</sub> and OH suggests that HO<sub>2</sub> leads to sink of C<sub>2</sub>F<sub>5</sub>CHO and C<sub>3</sub>H<sub>7</sub>CHO at night in these regions. In contrast, over oceanic regions like the Atlantic and Pacific, the [HO<sub>2</sub>]/[OH] ratios drop below 1, leading to a diminished role of HO<sub>2</sub> in these areas.

Our further analysis of the global distribution of the ratio between HO<sub>2</sub> and OH during daytime reveals that HO<sub>2</sub> concentrations are generally higher than those of OH (see Figure S4). Notably, along the west coast of South America (approximately between 0° and 30°S latitude and 60°W to 120°W longitude), the ratio can reach up to three orders of magnitude. Industrial areas (such as Russia and Malaysia) and certain regions in Africa also exhibit high ratios of 1-2 orders of magnitude. This suggests that in these areas, the concentration of HO<sub>2</sub> is significantly higher than that of OH, which may be related to local industrial activities or specific emission characteristics. However, due to the presence of daytime photolysis, the generation and loss pathways of HO<sub>2</sub> and OH become more complex, leading to significant uncertainty in interpreting the ratio. For instance, photolysis can alter the formation rates of HO<sub>2</sub> and OH, thereby affecting their concentration ratio. Additionally, the high ratios along the eastern coast of North America may be associated with atmospheric transport and regional emission features. Despite these complexities, the high daytime ratios still indicate that in specific regions, HO<sub>2</sub> may play a role in the oxidation pathways of C<sub>2</sub>F<sub>5</sub>CHO and C<sub>3</sub>H<sub>7</sub>CHO both during the day and at night. Future research should integrate observational data with model refinements to better quantify the impact of photolysis on the HO<sub>2</sub>/OH ratio.

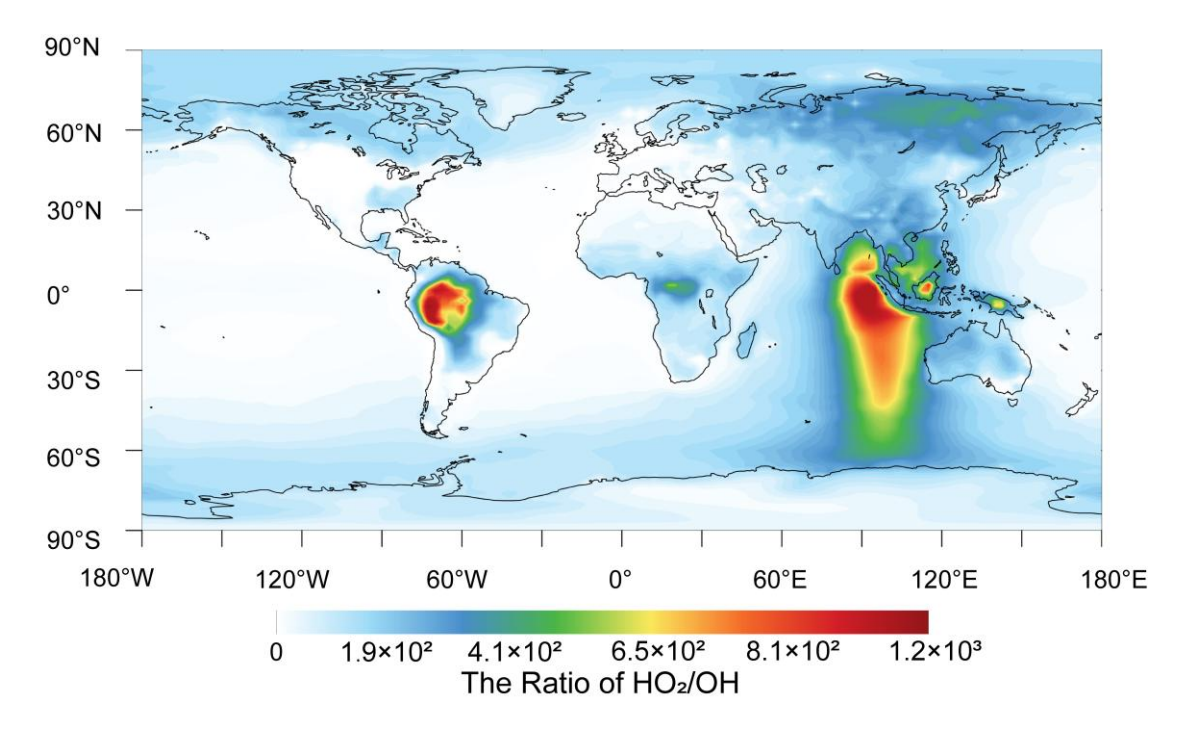
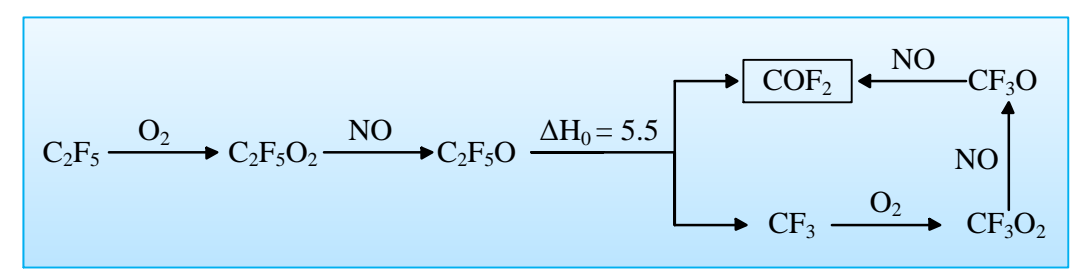


Figure 9. The annual average ratio of HO<sub>2</sub>/OH at night globally.

Moreover, except for generating formic acid, another intermediate product  $C_nF_{2n+1}$  can undergo a single-carbon shortening process as depicted in Figure 10 to ultimately convert into the more stable COF<sub>2</sub>. Taking the example of  $C_2F_5$ , the process starts with  $C_2F_5$  reacting with  $O_2$  to form  $C_2F_5O_2$ . Subsequently,  $C_2F_5O_2$  reacts with NO to produce  $C_2F_5O$ , which then undergoes C-C bond cleavage to generate  $CF_3$  and  $COF_2$ . The  $CF_3$  further reacts to eventually yield  $COF_2$  through a similar reaction pathway. However, the absence of quantified rate constants for these reactions prevents a robust assessment of their global or regional impacts. A comprehensive evaluation of the role of NO would require integrating the kinetics of  $RO_2 + RO_3$  reactions (e.g.,  $RO_3 + RO_3$ ) into atmospheric models, which is beyond the scope of this study.



**Figure 10.** Atmospheric degradation mechanism for  $C_nF_{2n+1}$  with  $C_2F_5$  used as a representative example.

In current studies, we focus on the homogeneous reactions of HO<sub>2</sub>-initiated linear perfluoroaldehydes. It is worth noting that the concentration of HO<sub>2</sub> at interfaces may be higher than in the gas phase, according to research findings. (Angelaki et al., 2024; Li et al., 2023) Given the strong reactivity at the water-air interface and the complex interplay and competition between

OH and HO<sub>2</sub>, the degradation of perfluoroaldehydes initiated by HO<sub>2</sub> and their potential contribution to atmospheric acidity may have a more pronounced impact. For example, Xia et al. (2024) recently reported the single-carbon and double-carbon pathways presented during the degradation of C<sub>7</sub>F<sub>15</sub> on the surface of water droplets. These heterogeneous reactions may also contribute to the removal of perfluoroaldehydes and the degradation process of polyfluoroalkyl substances. Nevertheless, further kinetics and mechanism are still required as a basis and support, so as to enable a more accurate and comprehensive understanding of this complex chemical process and its impact on atmospheric chemistry.

## 4. Summarizing Remarks

345

350

355

360

365

370

In this study, we have delved into the chemical reaction kinetics of linear perfluorinated aldehydes (C<sub>2</sub>F<sub>5</sub>CHO and C<sub>3</sub>F<sub>7</sub>CHO) with hydroperoxyl radicals in the gas phase using ab initio calculation methods and reaction kinetics theory. We find that the activation enthalpies for the reactions of C<sub>2</sub>F<sub>5</sub>CHO and C<sub>3</sub>F<sub>7</sub>CHO with HO<sub>2</sub> at 0 K are both -2.7 kcal/mol, demonstrating that carbon chain elongation in linear perfluoroaldehydes has a negligible thermodynamic influence on their enthalpies of activation at 0 K. This is further shown in C<sub>4</sub>F<sub>9</sub>CHO and C<sub>5</sub>F<sub>11</sub>CHO with HO<sub>2</sub>.

Further kinetic studies reveal that anharmonicity have a significant impact on the reaction rates, while the torsional anharmonicity, recross coefficient, and tunnelling effects contribute relatively little to the rate constants. It is particularly noteworthy that the reaction of  $C_3F_7CHO$  with  $HO_2$  exhibits a distinct pressure dependence, whereas the reaction of  $C_2F_5CHO$  with  $HO_2$  does not show such a pressure effect.

By integrating kinetics with the data based on GEOS-Chem modelling, we have identified some regions such as Russia, Malaysia, and parts of Africa, where HO<sub>2</sub> concentration exceeds OH concentration by 2–3 orders of magnitude. Therefore, the reactions of HO<sub>2</sub> with C<sub>2</sub>F<sub>5</sub>CHO and C<sub>3</sub>F<sub>7</sub>CHO can compete well with their corresponding reaction with OH. Specifically, the atmospheric lifetimes of C<sub>2</sub>F<sub>5</sub>CHO and C<sub>3</sub>F<sub>7</sub>CHO via HO<sub>2</sub> are shortened to be 14.4–31.3 h and 21.6–51.8 h, respectively, with orders of magnitude shorter than that of the corresponding OH-mediated pathways (>20 days). Under high NO<sub>x</sub> conditions, this pathway may contribute to tropospheric HCOOH and COF<sub>2</sub> formation.

While the present investigation establishes the HO<sub>2</sub>-mediated degradation pathway for linear perfluoroaldehydes (C<sub>2</sub>F<sub>5</sub>CHO/C<sub>3</sub>F<sub>7</sub>CHO), it simultaneously highlights critical gaps in our understanding of their atmospheric lifetimes. Notably, the current work focuses on gas-phase HO<sub>2</sub> reactions. However, the roles of heterogeneous interfacial processes (e.g., on aerosol surfaces or cloud droplets) remains unexplored.(Zhang et al., 2024b) The potential for HO<sub>2</sub>-driven defluorination to generate reactive CF<sub>3</sub> radicals, which could initiate secondary reactions (e.g., with O<sub>3</sub> or NO<sub>2</sub>), requires systematic investigation to assess implications for atmospheric oxidizing capacity and secondary aerosol formation. Additionally, the study focuses on radical-driven pathways but acknowledges that photolysis is a competing sink for linear perfluoroaldehydes. Future work should quantify photolysis rates under stratospheric UV conditions (e.g., 200–300 nm) to reconcile discrepancies between modeled and observed atmospheric lifetimes.(Thomson et al., 2025) Addressing these limitations will require integrating advanced experimental techniques (e.g., synchrotron-based photoionization mass spectrometry) with multi-scale modeling

frameworks, while prioritizing under sampled environments like the upper troposphere and polar regions where HO<sub>2</sub> reactivity anomalies could profoundly alter PFAS degradation trajectories.(Alam et al., 2024; Zhou et al., 2024b) Such efforts are critical for refining environmental risk assessments of emerging HFOs and guiding the design of next-generation chemicals with minimized atmospheric persistence.

# **Supplementary Material**

Separate document

## 380 Author contributions.

BL designed the project; ZGD performed the quantum chemical calculations; CLX performed the model calculations; ZGD, CLX, and BL analysed the data; ZGD wrote the manuscript draft. ZGD, CLX, and BL reviewed and edited the manuscript.

## **Competing interests**

The authors declare that they have no conflict of interest.

# 385 Financial support

This work was supported in part by the National Natural Science Foundation of China (42120104007 and 41775125) and by Guizhou Provincial Science and Technology Projects, China (ZK [2022]194, CXTD [2022]001, and GCC [2023]026).

## Reference

Ackerman Grunfeld, D., Gilbert, D., Hou, J., Jones, A. M., Lee, M. J., Kibbey, T. C. G., and O'Carroll, D. M.: Underestimated burden of per- and polyfluoroalkyl substances in global surface waters and groundwaters, Nature Geoscience, 17, 340–346, https://doi.org/10.1038/s41561-024-01402-8, 2024.

Adler, T. B., Knizia, G., and Werner, H. J.: A simple and efficient CCSD(T)-F12 approximation, Journal of Chemical Physics, 127, 221106, https://doi.org/10.1063/1.2817618, 2007.

Alam, M. S., Abbasi, A., and Chen, G.: Fate, distribution, and transport dynamics of Per- and Polyfluoroalkyl Substances (PFASs) in the environment, Journal of Environmental Management, 371, 123163, https://doi.org/10.1016/j.jenvman.2024.123163, 2024.

Andersen, M. P. S., Nielsen, O. J., Hurley, M. D., Ball, J. C., Wallington, T. J., Stevens, J. E., Martin, J. W., Ellis, D. A., and Mabury, S. A.: Atmospheric chemistry of n- $C_xF_{2x+1}$ CHO (x = 1, 3, 4): Reaction with Cl atoms, OH radicals and IR spectra of  $C_xF_{2x+1}$ C(O)O<sub>2</sub>NO<sub>2</sub>, Journal of Physical Chemistry A, 108, 5189–5196, https://doi.org/10.1021/jp0496598, 2004.

- Andersen, S. T., McGillen, M. R., Xue, C., Seubert, T., Dewald, P., Türk, G. N. T. E., Schuladen, J., Denjean, C., Etienne, J., Garrouste, O., Jamar, M., Harb, S., Cirtog, M., Michoud, V., Cazaunau, M., Bergé, A., Cantrell, C., Dusanter, S., Picquet-Varrault, B., Kukui, A., Mellouki, A., Carpenter, L. J., Lelieveld, J., and Crowley, J. N.: Measurement report: Sources, sinks, and lifetime of NO<sub>x</sub> in a suburban temperate forest at night, Atmospheric Chemistry and Physics, 24, 11603–11618, https://doi.org/10.5194/acp-24-11603-2024, 2024.
- Angelaki, M., Carreira Mendes Da Silva, Y., Perrier, S., and George, C.: Quantification and Mechanistic Investigation of the Spontaneous H<sub>2</sub>O<sub>2</sub> Generation at the Interfaces of Salt-Containing Aqueous Droplets, Journal of the American Chemical Society, 146, 8327–8334, https://doi.org/10.1021/jacs.3c14040, 2024.
  - Antiñolo, M., González, S., Ballesteros, B., Albaladejo, J., and Jiménez, E.: Laboratory studies of CHF<sub>2</sub>CF<sub>2</sub>CH<sub>2</sub>OH and CF <sub>3</sub>CF<sub>2</sub>CH<sub>2</sub>OH: UV and IR absorption cross sections and OH rate coefficients between 263 and 358 K, Journal of Physical
- Chemistry A, 116, 6041–6050, https://doi.org/10.1021/jp2111633, 2012.
  Antiñolo, M., Jiménez, E., González, S., and Albaladejo, J.: Atmospheric chemistry of CF<sub>3</sub>CF<sub>2</sub>CHO: Absorption cross sections in the UV and IR regions, photolysis at 308 nm, and gas-phase reaction with OH radicals (T = 263-358 K), Journal of Physical
- Bao, J. L. and Truhlar, D. G.: Variational transition state theory: Theoretical framework and recent developments, Chemical Society Reviews, 46, 7548–7596, https://doi.org/10.1039/c7cs00602k, 2017.

Chemistry A, 118, 178–186, https://doi.org/10.1021/jp410283v, 2014.

- Bao, J. L., Zheng, J., and Truhlar, D. G.: Kinetics of Hydrogen Radical Reactions with Toluene Including Chemical Activation Theory Employing System-Specific Quantum RRK Theory Calibrated by Variational Transition State Theory, Journal of the American Chemical Society, 138, 2690–2704, https://doi.org/10.1021/jacs.5b11938, 2016a.
- Bao, J. L., Zhang, X., and Truhlar, D. G.: Predicting pressure-dependent unimolecular rate constants using variational transition state theory with multidimensional tunneling combined with system-specific quantum RRK theory: A definitive test for fluoroform dissociation, Physical Chemistry Chemical Physics, 18, 16659–16670, https://doi.org/10.1039/c6cp02765b, 2016b. Berndt, T., Richters, S., Kaethner, R., Voigtländer, J., Stratmann, F., Sipilä, M., Kulmala, M., and Herrmann, H.: Gas-Phase Ozonolysis of Cycloalkenes: Formation of Highly Oxidized RO<sub>2</sub> Radicals and Their Reactions with NO, NO<sub>2</sub>, SO<sub>2</sub>, and Other RO<sub>2</sub> Radicals, Journal of Physical Chemistry A, 119, 10336–10348, https://doi.org/10.1021/acs.jpca.5b07295, 2015.
- Bey, I., Jacob, D. J., Yantosca, R. M., Logan, J. A., Field, B. D., Fiore, A. M., Li, Q., Liu, H. Y., Mickley, L. J., and Schultz, M. G.: Global modeling of tropospheric chemistry with assimilated meteorology: Model description and evaluation, Journal of Geophysical Research Atmospheres, 106, 23073–23095, https://doi.org/10.1029/2001JD000807, 2001.
  - Bloino, J., Biczysko, M., and Barone, V.: General perturbative approach for spectroscopy, thermodynamics, and kinetics: Methodological background and benchmark studies, Journal of Chemical Theory and Computation, 8, 1015–1036, https://doi.org/10.1021/ct200814m, 2012.
  - Bloss, W. J., Lee, J. D., Heard, D. E., Salmon, R. A., Bauguitte, S. J. B., Roscoe, H. K., and Jones, A. E.: Observations of OH and HO<sub>2</sub> radicals in coastal Antarctica, Atmospheric Chemistry and Physics, 7, 4171–4185, https://doi.org/10.5194/acp-7-4171-2007, 2007.

- Bottorff, B., Lew, M. M., Woo, Y., Rickly, P., Rollings, M. D., Deming, B., Anderson, D. C., Wood, E., Alwe, H. D., Millet,
- D. B., Weinheimer, A., Tyndall, G., Ortega, J., Dusanter, S., Leonardis, T., Flynn, J., Erickson, M., Alvarez, S., Rivera-Rios, J. C., Shutter, J. D., Keutsch, F., Helmig, D., Wang, W., Allen, H. M., Slade, J. H., Shepson, P. B., Bertman, S., and Stevens, P. S.: OH, HO<sub>2</sub>, and RO<sub>2</sub> radical chemistry in a rural forest environment: measurements, model comparisons, and evidence of a missing radical sink, Atmospheric Chemistry and Physics, 23, 10287–10311, https://doi.org/10.5194/acp-23-10287-2023,
- Brasseur, G. and Solomon, S.: Aeronomy of the middle atmosphere: chemistry and physics of the stratosphere and mesosphere., Springer Science & Business Media, 617–627 pp., https://doi.org/10.1007/1-4020-3824-0, 2006.

2023.

455

- Burkholder, J. B., Cox, R. A., and Ravishankara, A. R.: Atmospheric Degradation of Ozone Depleting Substances, Their Substitutes, and Related Species, Chemical Reviews, 115, 3704–3759, https://doi.org/10.1021/cr5006759, 2015.
- Canneaux, S., Bohr, F., and Henon, E.: KiSThelP: A program to predict thermodynamic properties and rate constants from
- quantum chemistry results, Journal of Computational Chemistry, 35, 82–93, https://doi.org/10.1002/jcc.23470, 2014.
  Chen, W., Zheng, J., Bao, J. L., Truhlar, D. G., and Xu, X.: MSTor 2023: A new version of the computer code for multistructural torsional anharmonicity, now with automatic torsional identification using redundant internal coordinates, Computer Physics Communications, 288, 108740, https://doi.org/10.1016/j.cpc.2023.108740, 2023.
  - Chiappero, M. S., Malanca, F. E., Argüello, G. A., Wooldridge, S. T., Hurley, M. D., Ball, J. C., Wallington, T. J., Waterland,
- 450 R. L., and Buck, R. C.: Atmospheric chemistry of perfluoroaldehydes (C<sub>x</sub>F<sub>2x+1</sub>CHO) and fluorotelomer aldehydes (C<sub>x</sub>F<sub>2x+1</sub>CH<sub>2</sub>CHO): Quantification of the important role, of photolysis, Journal of Physical Chemistry A, 110, 11944–11953, https://doi.org/10.1021/jp064262k, 2006.
  - Chiappero, M. S., Argüello, G. A., Hurley, M. D., and Wallington, T. J.: Atmospheric chemistry of  $n-C_6F_{13}CH_2CHO$ : Formation from  $n-C_6F_{13}CH_2CH_2OH$ , kinetics, and mechanisms of reactions with chlorine atoms and OH radicals, Journal of
- David, L. M., Barth, M., Höglund-Isaksson, L., Purohit, P., Velders, G. J. M., Glaser, S., and Ravishankara, A. R.: Trifluoroacetic acid deposition from emissions of HFO-1234yf in India, China, and the Middle East, Atmospheric Chemistry and Physics, 21, 14833–14849, https://doi.org/10.5194/acp-21-14833-2021, 2021.

Physical Chemistry A, 114, 6131–6137, https://doi.org/10.1021/jp101587m, 2010.

- Ding, D. P. and Long, B.: Reaction between propional dehyde and hydroxyperoxy radical in the atmosphere: A reaction route for the sink of propional dehyde and the formation of formic acid, Atmospheric Environment, 284, 119202, https://doi.org/10.1016/j.atmosenv.2022.119202, 2022.
  - Dong, Z. G., Xu, F., Mitchell, E., and Long, B.: Trifluoroacetaldehyde aminolysis catalyzed by a single water molecule: An important sink pathway for trifluoroacetaldehyde and a potential pathway for secondary organic aerosol growth, Atmospheric Environment, 249, 118242, https://doi.org/10.1016/j.atmosenv.2021.118242, 2021.
- Gao, Q., Shen, C., Zhang, H., Long, B., and Truhlar, D. G.: Quantitative Kinetics Reveal that Reactions of HO<sub>2</sub> are a Significant Sink for Aldehydes in the Atmosphere and may Initiate the Formation of Highly Oxygenated Molecules via Autoxidation, Physical Chemistry Chemical Physics, 26, 16160–16174, https://doi.org/10.1039/d4cp00693c, 2024a.

- Gao, Q., Shen, C., Zhang, H., Long, B., and Truhlar, D. G.: Quantitative kinetics reveal that reactions of HO<sub>2</sub> are a significant sink for aldehydes in the atmosphere and may initiate the formation of highly oxygenated molecules via autoxidation, Physical
- 470 Chemistry Chemical Physics, 26, 16160–16174, https://doi.org/10.1039/d4cp00693c, 2024b.
  - Garrett, B. C. and Truhlar, D. G.: Criterion of minimum state density in the transition state theory of bimolecular reactions, The Journal of Chemical Physics, 70, 1593–1598, https://doi.org/10.1063/1.437698, 1979.
    - Gelaro, R., McCarty, W., Suárez, M. J., Todling, R., Molod, A., Takacs, L., Randles, C. A., Darmenov, A., Bosilovich, M. G., Reichle, R., Wargan, K., Coy, L., Cullather, R., Draper, C., Akella, S., Buchard, V., Conaty, A., da Silva, A. M., Gu, W., Kim,
- G. K., Koster, R., Lucchesi, R., Merkova, D., Nielsen, J. E., Partyka, G., Pawson, S., Putman, W., Rienecker, M., Schubert, S. D., Sienkiewicz, M., and Zhao, B.: The modern-era retrospective analysis for research and applications, version 2 (MERRA-2), Journal of Climate, 30, 5419–5454, https://doi.org/10.1175/JCLI-D-16-0758.1, 2017.
  - Goldman, M. J., Green, W. H., and Kroll, J. H.: Chemistry of Simple Organic Peroxy Radicals under Atmospheric through Combustion Conditions: Role of Temperature, Pressure, and NO<sub>x</sub> Level, Journal of Physical Chemistry A, 125, 10303–10314,
- 480 https://doi.org/10.1021/acs.jpca.1c07203, 2021.
  - Gyevi-Nagy, L., Kállay, M., and Nagy, P. R.: Accurate Reduced-Cost CCSD(T) Energies: Parallel Implementation, Benchmarks, and Large-Scale Applications, Journal of Chemical Theory and Computation, 17, 860–878, https://doi.org/10.1021/acs.jctc.0c01077, 2021.
- Hermans, I., Müller, J. F., Nguyen, T. L., Jacobs, P. A., and Peeters, J.: Kinetics of α-Hydroxy-alkylperoxyl radicals in oxidation processes. HO<sub>2</sub>-Initiated oxidation of ketones/aldehydes near the tropopause, Journal of Physical Chemistry A, 109, 4303–4311, https://doi.org/10.1021/jp044080v, 2005.
  - Hratchian, H. P. and Schlegel, H. B.: Accurate reaction paths using a Hessian based predictor-corrector integrator, Journal of Chemical Physics, 120, 9918–9924, https://doi.org/10.1063/1.1724823, 2004.
  - Hratchian, H. P. and Schlegel, H. B.: Using Hessian Updating To Increase the Efficiency of a Hessian Based Predictor-
- Corrector Reaction Path Following Method, Journal of Chemical Theory and Computation, 1, 61–69, 2005.
   Hu, L., Millet, D. B., Baasandorj, M., Griffis, T. J., Turner, P., Helmig, D., Curtis, A. J., and Hueber, J.: Isoprene emissions and impacts over an ecological transition region in the U.S. Upper Midwest inferred from tall tower measurements, Journal of

Geophysical Research: Atmospheres, 120, 3553–3571, https://doi.org/https://doi.org/10.1002/2014JD022732, 2015.

- Hurley, M. D., Wallington, T. J., Sulbaek Andersen, M. P., Ellis, D. A., Martin, J. W., and Mabury, S. A.: Atmospheric chemistry of fluorinated alcohols: Reaction with Cl atoms and OH radicals and atmospheric lifetimes, Journal of Physical
- Chemistry A, 108, 1973–1979, https://doi.org/10.1021/jp0373088, 2004. Hurley, M. D., Ball, J. C., Wallington, T. J., Sulbaek Andersen, M. P., Nielsen, C. J., Ellis, D. A., Martin, J. W., and Mabury, S. A.: Atmospheric chemistry of  $n-C_xF_{2x+1}CHO$  (x=1,2,3,4): Fate of  $n-C_xF_{2x+1}C(O)$  radicals, Journal of Physical Chemistry A, 110, 12443–12447, 2006.
- Jiménez, E., González, S., Cazaunau, M., Chen, H., Ballesteros, B., Daële, V., Albaladejo, J., and Mellouki, A.: Atmospheric Degradation Initiated by OH Radicals of the Potential Foam Expansion Agent, CF<sub>3</sub>(CF<sub>2</sub>)<sub>2</sub>CH=CH<sub>2</sub> (HFC-1447fz): Kinetics

- and Formation of Gaseous Products and Secondary Organic Aerosols, Environmental Science and Technology, 50, 1234–1242, https://doi.org/10.1021/acs.est.5b04379, 2016.
- Kállay, M., Nagy, P. R., Mester, D., Rolik, Z., Samu, G., Csontos, J., Csóka, J., Szabó, P. B., Gyevi-Nagy, L., Hégely, B.,
- Ladjánszki, I., Szegedy, L., Ladóczki, B., Petrov, K., Farkas, M., Mezei, P. D., and Ganyecz, Á.: The MRCC program system: Accurate quantum chemistry from water to proteins., The Journal of chemical physics, 152, 74107, https://doi.org/10.1063/1.5142048, 2020.
  - Kelly, T., Sidebottom, H., Nielsen, C. J., and Sellevag, S. R.: A study of the IR and UV-Vis absorption cross-sections, photolysis and OH-initiated oxidation of CF<sub>3</sub>CHO and CF<sub>3</sub>CH<sub>2</sub>CHO, Physical Chemistry Chemical Physics, 1243–1252, 2004.
- 510 Kenyon, R. L.: The Path of Chemical Reactions—The IRC Approach, Accounts of Chemical Research, 46, 5, https://doi.org/10.1021/cen-v046n004.p005, 1968.
  - King, M. D., Canosa-Mas, C. E., and Wayne, R. P.: Gas-phase reactions between RO<sub>2</sub> and NO, HO<sub>2</sub> or CH<sub>3</sub>O<sub>2</sub>: correlations between rate constants and the SOMO energy of the peroxy (RO<sub>2</sub>) radical, Atmospheric Environment, 35, 2081–2088, https://doi.org/10.1016/S1352-2310(00)00501-X, 2001.
- Knizia, G., Adler, T. B., and Werner, H. J.: Simplified CCSD(T)-F12 methods: Theory and benchmarks, Journal of Chemical Physics, 130, 054104, https://doi.org/10.1063/1.3054300, 2009.
  - Kuhler, K. M., Truhlar, D. G., and Isaacson, A. D.: General method for removing resonance singularities in quantum mechanical perturbation theory, The Journal of Chemical Physics, 104, 4664–4671, https://doi.org/10.1063/1.471161, 1996.
  - Lee, B. H., Munger, J. W., Wofsy, S. C., Rizzo, L. V., Yoon, J. Y. S., Turner, A. J., Thornton, J. A., and Swann, A. L. S.:
- Sensitive Response of Atmospheric Oxidative Capacity to the Uncertainty in the Emissions of Nitric Oxide (NO) From Soils in Amazonia, Geophysical Research Letters, 51, e2023GL107214, https://doi.org/10.1029/2023GL107214, 2024.
  - Lelieveld, J., Gromov, S., Pozzer, A., and Taraborrelli, D.: Global tropospheric hydroxyl distribution, budget and reactivity, Atmospheric Chemistry and Physics, 16, 12477–12493, https://doi.org/10.5194/acp-16-12477-2016, 2016.
  - Lew, M. M., Rickly, P. S., Bottorff, B. P., Reidy, E., Sklaveniti, S., Léonardis, T., Locoge, N., Dusanter, S., Kundu, S., Wood,
- 525 E., and Stevens, P. S.: OH and HO<sub>2</sub> radical chemistry in a midlatitude forest: Measurements and model comparisons, Atmospheric Chemistry and Physics, 20, 9209–9230, https://doi.org/10.5194/acp-20-9209-2020, 2020.
  - Li, K., Guo, Y., Nizkorodov, S. A., Rudich, Y., Angelaki, M., Wang, X., An, T., Perrier, S., and George, C.: Spontaneous dark formation of OH radicals at the interface of aqueous atmospheric droplets, Proceedings of the National Academy of Sciences, 120, e2220228120, https://doi.org/10.1073/pnas, 2023a.
- Li, K., Guo, Y., Nizkorodov, S. A., Rudich, Y., Angelaki, M., Wang, X., An, T., Perrier, S., and George, C.: Spontaneous dark formation of OH radicals at the interface of aqueous atmospheric droplets, Proceedings of the National Academy of Sciences of the United States of America, 120, e2220228120, https://doi.org/10.1073/pnas.2220228120, 2023b.
  - Li, X., Wang, Y., Cui, J., Shi, Y., and Cai, Y.: Occurrence and Fate of Per- and Polyfluoroalkyl Substances (PFAS) in Atmosphere: Size-Dependent Gas-Particle Partitioning, Precipitation Scavenging, and Amplification, Environmental Science
- 535 and Technology, 58, 9283–9291, https://doi.org/10.1021/acs.est.4c00569, 2024.

- Lin, H., Jacob, D. J., Lundgren, E. W., Sulprizio, M. P., Keller, C. A., Fritz, T. M., Eastham, S. D., Emmons, L. K., Campbell, P. C., Baker, B., Saylor, R. D., and Montuoro, R.: Harmonized Emissions Component (HEMCO) 3.0 as a versatile emissions component for atmospheric models: Application in the GEOS-Chem, NASA GEOS, WRF-GC, CESM2, NOAA GEFS-Aerosol, and NOAA UFS models, Geoscientific Model Development, 14, 5487–5506, https://doi.org/10.5194/gmd-14-5487-2021, 2021.
- Liu, Y. P., Lynch, G. C., Truong, T. N., Lu, D. hong, Truhlar, D. G., and Garrett, B. C.: Molecular Modeling of the Kinetic Isotope Effect for the [1,5] Sigmatropic Rearrangement of cis-1,3-Pentadiene, Journal of the American Chemical Society, 115, 2408–2415, https://doi.org/10.1021/ja00059a041, 1993.
- Long, B., Bao, J. L., and Truhlar, D. G.: Atmospheric Chemistry of Criegee Intermediates: Unimolecular Reactions and Reactions with Water, Journal of the American Chemical Society, 138, 14409–14422, https://doi.org/10.1021/jacs.6b08655, 2016.

- Long, B., Bao, J. L., and Truhlar, D. G.: Rapid unimolecular reaction of stabilized Criegee intermediates and implications for atmospheric chemistry, Nature Communications, 10, 2003, https://doi.org/10.1038/s41467-019-09948-7, 2019.
- Long, B., Xia, Y., and Truhlar, D. G.: Quantitative Kinetics of HO<sub>2</sub> Reactions with Aldehydes in the Atmosphere: High-Order Dynamic Correlation, Anharmonicity, and Falloff Effects Are All Important, Journal of the American Chemical Society, 144, 19910–19920, https://doi.org/10.1021/jacs.2c07994, 2022.
  - Long, B., Zhang, Y.-Q., Xie, C., Tan, X.-F., and Truhlar, D. G.: Reaction of Carbonyl Oxide with Hydroperoxymethyl Thioformate: Quantitative Kinetics and Atmospheric Implications, Research, 7, 525, https://doi.org/10.34133/research.0525, 2024.
- Lynch, B. J., Zhao, Y., and Truhlar, D. G.: Effectiveness of diffuse basis functions for calculating relative energies by density functional theory, Journal of Physical Chemistry A, 107, 1384–1388, https://doi.org/10.1021/jp021590l, 2003.
  M. Kállay, P. R. Nagy, D. Mester, L. Gyevi-Nagy, J. Csóka, P. B. Szabó, Z. Rolik, G. Samu, J. Csontos, B. Hégely, Á. Ganyecz, I. Ladjánszki, L. Szegedy, B. Ladóczki, K. Petrov, M. Farkas, P. D. Mezei, R. A. H.: MRCC, a quantum chemical program suite, 2022.
- Martin, J. W., Mabury, S. A., and O'Brien, P. J.: Metabolic products and pathways of fluorotelomer alcohols in isolated rat hepatocytes, Chemico-Biological Interactions, 155, 165–180, https://doi.org/10.1016/j.cbi.2005.06.007, 2005.
   McDuffie, E. E., Smith, S. J., O'Rourke, P., Tibrewal, K., Venkataraman, C., Marais, E. A., Zheng, B., Crippa, M., Brauer, M., and Martin, R. V.: A global anthropogenic emission inventory of atmospheric pollutants from sector- And fuel-specific sources (1970-2017): An application of the Community Emissions Data System (CEDS), Earth System Science Data, 12, 3413–3442, https://doi.org/10.5194/essd-12-3413-2020, 2020.
  - Nie, W., Yan, C., Yang, L., Roldin, P., Liu, Y., Vogel, A. L., Molteni, U., Stolzenburg, D., Finkenzeller, H., Amorim, A., Bianchi, F., Curtius, J., Dada, L., Draper, D. C., Duplissy, J., Hansel, A., He, X. C., Hofbauer, V., Jokinen, T., Kim, C., Lehtipalo, K., Nichman, L., Mauldin, R. L., Makhmutov, V., Mentler, B., Mizelli-Ojdanic, A., Petäjä, T., Quéléver, L. L. J., Schallhart, S., Simon, M., Tauber, C., Tomé, A., Volkamer, R., Wagner, A. C., Wagner, R., Wang, M., Ye, P., Li, H., Huang,

- W., Qi, X., Lou, S., Liu, T., Chi, X., Dommen, J., Baltensperger, U., El Haddad, I., Kirkby, J., Worsnop, D., Kulmala, M., Donahue, N. M., Ehn, M., and Ding, A.: NO at low concentration can enhance the formation of highly oxygenated biogenic molecules in the atmosphere, Nature Communications, 14, 3347, https://doi.org/10.1038/s41467-023-39066-4, 2023.
  Orlando, J. J., Iraci, L. T., and Tyndall, G. S.: Chemistry of the cyclopentoxy and cyclohexoxy radicals at subambient temperatures, Journal of Physical Chemistry A, 104, 5072–5079, https://doi.org/10.1021/jp0002648, 2000.
- 575 Rand, A. A. and Mabury, S. A.: Is there a human health risk associated with indirect exposure to perfluoroalkyl carboxylates (PFCAs)?, Toxicology, 375, 28–36, https://doi.org/10.1016/j.tox.2016.11.011, 2017. Rupp, J., Guckert, M., Berger, U., Drost, W., Mader, A., Nödler, K., Nürenberg, G., Schulze, J., Söhlmann, R., and Reemtsma, T.: Comprehensive target analysis and TOP assay of per- and polyfluoroalkyl substances (PFAS) in wild boar livers indicate contamination hot-spots in the environment. Science of the Total Environment. 871. 162028. 580 https://doi.org/10.1016/j.scitotenv.2023.162028, 2023.
- Sascha, A. R., Novelli, A., Hofzumahaus, A., Kang, S., Baker, Y., Mentel, T., Wahner, A., and Fuchs, H.: Measurements of hydroperoxy radicals (HO<sub>2</sub>) at atmospheric concentrations using bromide chemical ionisation mass spectrometry, Atmospheric Measurement Techniques, 12, 891–902, https://doi.org/10.5194/amt-12-891-2019, 2019.
- Solignac, G., Mellouki, A., Le Bras, G., Yujing, M., and Sidebottom, H.: The gas phase tropospheric removal of fluoroaldehydes (C<sub>x</sub>F<sub>2x+1</sub>CHO, x=3,4,6), Physical Chemistry Chemical Physics, 9, 4200–4210, https://doi.org/10.1039/b614502g, 2007.
  - Sulbaek Andersen, M. P., Hurley, M. D., Wallington, T. J., Ball, J. C., Martin, J. W., Ellis, D. A., Mabury, S. A., and Nielsen, O. J.: Atmospheric chemistry of C<sub>2</sub>F<sub>5</sub>CHO: Reaction with Cl atoms and OH radicals, IR spectrum of C<sub>2</sub>F<sub>5</sub>C(O)O<sub>2</sub>NO<sub>2</sub>, Chemical Physics Letters, 379, 28–36, https://doi.org/10.1016/j.cplett.2003.08.004, 2003.
- 590 Sznajder-Katarzyńska, K., Surma, M., and Cieślik, I.: A Review of Perfluoroalkyl Acids (PFAAs) in terms of Sources, Applications, Human Exposure, Dietary Intake, Toxicity, Legal Regulation, and Methods of Determination, Journal of Chemistry, 2019, 2717528, https://doi.org/10.1155/2019/2717528, 2019.
  - Taube, A. G. and Bartlett, R. J.: Frozen natural orbital coupled-cluster theory: Forces and application to decomposition of nitroethane, Journal of Chemical Physics, 128, 164101, https://doi.org/10.1063/1.2902285, 2008.
- Thackray, C. P., Selin, N. E., and Young, C. J.: A global atmospheric chemistry model for the fate and transport of PFCAs and their precursors, Environmental Science: Processes and Impacts, 22, 285–293, https://doi.org/10.1039/c9em00326f, 2020.
  Thomson, A. J., Giannopoulos, G., Pretty, J., Baggs, E. M., and Richardson, D. J.: Biological sources and sinks of nitrous oxide and strategies to mitigate emissions, Philosophical Transactions of the Royal Society B: Biological Sciences, 367, 1157–1168, https://doi.org/10.1098/rstb.2011.0415, 2012.
- Thomson, J. D., Campbell, J. S., Edwards, E. B., Medcraft, C., Nauta, K., Pérez-Peña, M. P., Fisher, J. A., Osborn, D. L., Kable, S. H., and Hansen, C. S.: Fluoroform (CHF<sub>3</sub>) Production from CF<sub>3</sub>CHO Photolysis and Implications for the Decomposition of Hydrofluoroolefins and Hydrochlorofluoroolefins in the Atmosphere, Journal of the American Chemical Society, 147, 33–38, https://doi.org/10.1021/jacs.4c11776, 2025.

- Truhlar, D. G., Isaacson, A. D., Skodje, R. T., and Garrett, B. C.: Incorporation of quantum effects in generalized-transition-state theory. Journal of Physical Chemistry, 86, 2252–2261, https://doi.org/10.1021/i100209a021, 1982.
  - Vereecken, L. and Peeters, J.: Decomposition of substituted alkoxy radicals-Part I: A generalized structure-activity relationship for reaction barrier heights, Physical Chemistry Chemical Physics, 11, 9062–9074, https://doi.org/10.1039/b909712k, 2009.
  - Wang, Y., Liu, J. yao, Yang, L., Zhao, X. lei, Ji, Y. M., and Li, Z. sheng: Theoretical studies and rate constant calculations of the reactions  $C_2F_5$ CHO with OH radicals and Cl atoms, Journal of Molecular Structure: THEOCHEM, 820, 26–34,
- 610 https://doi.org/10.1016/j.theochem.2007.06.001, 2007.
  - Wang, Y., Wang, Z., Sun, M., Guo, J., and Zhang, J.: Emissions, degradation and impact of HFO-1234ze from China PU foam industry, Science of the Total Environment, 780, 146631, https://doi.org/10.1016/j.scitotenv.2021.146631, 2021.
  - Wang, Y., Liu, L., Qiao, X., Sun, M., Guo, J., Zhao, B., and Zhang, J.: Atmospheric fate and impacts of HFO-1234yf from mobile air conditioners in East Asia, Science of the Total Environment, 916, 170137,
- 615 https://doi.org/10.1016/j.scitotenv.2024.170137, 2024.

- Wang, Y., Liu, L., Qiao, X., Sun, M., Guo, J., Zhang, J., and Zhao, B.: Projections of National-Gridded Emissions of Hydrofluoroolefins (HFOs) in China, Environmental Science and Technology, 57, 8650–8659, https://doi.org/10.1021/acs.est.2c09263, 2023.
- Waterland, R. L. and Dobbs, K. D.: Atmospheric chemistry of linear perfluorinated aldehydes: Dissociation kinetics of C<sub>n</sub>F<sub>2n+1</sub>CO radicals, Journal of Physical Chemistry A, 111, 2555–2562, https://doi.org/10.1021/jp067587+, 2007.
  - Werner, H.-J., Knowles, P. J., Knizia, G., Manby, F. R., Schütz, M., Celani, P., Györffy, W., Kats, D., Korona, T., Lindh, R., Mitrushenkov, A., Rauhut, G., Shamasundar, K. R., Adler, T. B., Amos, R. D., Bennie, S. J., Bernhardsson, A., Berning, A., Cooper, D. L., Deegan, M. J. O., Dobbyn, A. J., Eckert, F., Goll, E., Hampel, C., Hesselmann, A., Hetzer, G., Hrenar, T., Jansen, G., Köppl, C., Lee, S. J. R., Liu, Y., Lloyd, A. W., Ma, Q., Mata, R. A., May, A. J., McNicholas, S. J., Meyer, W.,
- Miller III, T. F., Mura, M. E., Nicklass, A., O'Neill, D. P., Palmieri, P., Peng, D., Pflüger, K., Pitzer, R., Reiher, M., Shiozaki, T., Stoll, H., Stone, A. J., Tarroni, R., Thorsteinsson, T., Wang, M., and Welborn, M.: MOLPRO, version 2019.2, a package of ab initio programs, 2019.
  - Wu, J., Zhuang, Y., Dong, B., Wang, F., Yan, Y., Zhang, D., Liu, Z., Duan, X., Bo, Y., and Peng, L.: Spatial heterogeneity of per- and polyfluoroalkyl substances caused by glacial melting in Tibetan Lake Nam Co due to global warming, Journal of Hazardous Materials, 478, 135468, https://doi.org/10.1016/j.jhazmat.2024.135468, 2024.
- Xia, D., Zhang, H., Ju, Y., Xie, H., Su, L., Ma, F., Jiang, J., Chen, J., and Francisco, J. S.: Spontaneous Degradation of the "Forever Chemicals" Perfluoroalkyl and Polyfluoroalkyl Substances (PFASs) on Water Droplet Surfaces, Journal of the American Chemical Society, 146, 11266–11271, https://doi.org/10.1021/jacs.4c00435, 2024.
  - Xia, Y., Long, B., Liu, A., and Truhlar, D. G.: Reactions with criegee intermediates are the dominant gas-phase sink for formyl
- 635 fluoride in the atmosphere, Fundamental Research, 4, 1216–1224, https://doi.org/10.1016/j.fmre.2023.02.012, 2024.

- Yu, T., Zheng, J., and Truhlar, D. G.: Multipath variational transition state theory: Rate constant of the 1,4-hydrogen shift isomerization of the 2-cyclohexylethyl radical, Journal of Physical Chemistry A, 116, 297–308, https://doi.org/10.1021/jp209146b, 2012.
- Yu, Y., Pan, L., Sun, Q., and Wang, J.: The mechanism and kinetics of the atmospheric oxidation of CF<sub>3</sub>(CF<sub>2</sub>)<sub>2</sub>CH=CH<sub>2</sub> (HFC-1447fz) by hydroxyl radicals: ab initio investigation, Physical Chemistry Chemical Physics, 26, 10989–10997, https://doi.org/10.1039/d3cp06149c, 2024.
  - Zhang, T., Zhang, Y., Wen, M., Tang, Z., Long, B., Yu, X., Zhao, C., and Wang, W.: Effects of water, ammonia and formic acid on HO<sub>2</sub> + Cl reactions under atmospheric conditions: Competition between a stepwise route and one elementary step, RSC Advances, 9, 21544–21556, https://doi.org/10.1039/c9ra03541a, 2019.
- Zhang, W., Issa, K., Tang, T., and Zhang, H.: Role of Hydroperoxyl Radicals in Heterogeneous Oxidation of Oxygenated Organic Aerosols, Environmental Science and Technology, 58, 4727–4736, https://doi.org/10.1021/acs.est.3c09024, 2024a. Zhang, W., Issa, K., Tang, T., and Zhang, H.: Role of Hydroperoxyl Radicals in Heterogeneous Oxidation of Oxygenated Organic Aerosols, Environmental Science & Technology, 58, 4727–4736, https://doi.org/10.1021/acs.est.3c09024, 2024b. Zhang, Y., Cheng, Y., Zhang, T., Wang, R., Ji, J., Xia, Y., Lily, M., Wang, Z., and Muthiah, B.: A computational study of the
- $650 \quad HO_2 + SO_3 \rightarrow HOSO_2 + 3O_2$  reaction catalyzed by a water monomer, a water dimer and small clusters of sulfuric acid: kinetics and atmospheric implications, Physical Chemistry Chemical Physics, 24, 18205–18216, https://doi.org/10.1039/d1cp03318b, 2022.
  - Zhao, Y. and Truhlar, D. G.: Exploring the limit of accuracy of the global hybrid meta density functional for main-group thermochemistry, kinetics, and noncovalent interactions, Journal of Chemical Theory and Computation, 4, 1849–1868,
- Zhao, Y. and Truhlar, D. G.: The M06 suite of density functionals for main group thermochemistry, thermochemical kinetics, noncovalent interactions, excited states, and transition elements: Two new functionals and systematic testing of four M06 functionals and 12 other functionals, Theoretical Chemistry Accounts, 119, 525, https://doi.org/10.1007/s00214-007-0401-8,

2008b.

https://doi.org/10.1021/ct800246v, 2008a.

- Zheng, J. and Truhlar, D. G.: Kinetics of hydrogen-transfer isomerizations of butoxyl radicals, Physical Chemistry Chemical Physics, 12, 7782–7793, https://doi.org/10.1039/b927504e, 2010.
  - Zheng, J. and Truhlar, D. G.: Quantum thermochemistry: Multistructural method with torsional anharmonicity based on a coupled torsional potential, Journal of Chemical Theory and Computation, 9, 1356–1367, https://doi.org/10.1021/ct3010722, 2013.
- Zheng, J., Yu, T., Papajak, E., Alecu, I. M., Mielke, S. L., and Truhlar, D. G.: Practical methods for including torsional anharmonicity in thermochemical calculations on complex molecules: The internal-coordinate multi-structural approximation, Physical Chemistry Chemical Physics, 13, 10885–10907, https://doi.org/10.1039/c0cp02644a, 2011.

- Zheng, J., Meana-Pañeda, R., and Truhlar, D. G.: Prediction of Experimentally Unavailable Product Branching Ratios for Biofuel Combustion: The Role of Anharmonicity in the Reaction of Isobutanol with OH, Journal of the American Chemical
- Zheng, J., Oyedepo, G. A., and Truhlar, D. G.: Kinetics of the Hydrogen Abstraction Reaction From 2-Butanol by OH Radical, The Journal of Physical Chemistry A, 119, 12182–12192, https://doi.org/10.1021/acs.jpca.5b06121, 2015.

Society, 136, 5150–5160, https://doi.org/10.1021/ja5011288, 2014.

- Zheng, J., Bao, J. L., Meana-Pañeda, R., Zhang, S., J.Lynch, B., Corchado, J. C., Chuang, Y., Fast, P. L., Hu, W.-P., Liu, Y.-P., Lynch, G. C., Nguyen, K. A., Jackels, C. F., Ramos, A. F., Ellingson, B. A., Melissas, V. S., Villà, J., Rossi, I., Coitiño, E.
- 675 L., Pu, J., Albu, T. V., Ratkiewicz, A., Steckler, R., Garrett, B. C., Isaacson, A. D., and Truhlar, D. G.: Polyrate-version 2017-C; University of Minnesota: Minneapolis, 2017.
  - Zheng, J., Bao, J. L., Zhang, S., Corchado, J. C., Chuang, Y., Ellingson, B. A., and Truhlar, D. G.: Gaussrate, version 2017-B; University of Minnesota: Minneapolis, MN, 2018., https://comp.chem.umn.edu/polyrate/.
  - Zhou, J., Fukusaki, Y., Murano, K., Gautam, T., Bai, Y., Inomata, Y., Komatsu, H., Takeda, M., Yuan, B., Shao, M., Sakamoto,
- 680 Y., and Kajii, Y.: Investigation of HO<sub>2</sub> uptake mechanisms onto multiple-component ambient aerosols collected in summer winter time in Yokohama, Japan, Journal of Environmental Sciences (China), 137, 18-29, and https://doi.org/10.1016/j.jes.2023.02.030, 2024a.
  - Zhou, Y., Wang, X., Wang, C., Ji, Z., Niu, X., and Dong, H.: Fate of 'forever chemicals' in the global cryosphere, Earth-Science Reviews, 259, 104973, https://doi.org/10.1016/j.earscirev.2024.104973, 2024b.
- Ziemann, P. J. and Atkinson, R.: Kinetics, products, and mechanisms of secondary organic aerosol formation, Chemical Society Reviews, 41, 6582–6605, https://doi.org/10.1039/c2cs35122f, 2012.